Rapport de stage individuel

5ème année

Analysis of morpho-sedimentary dynamics of a Mediterranean stream affected by human disturbance

Museo Nacional de Ciencias Naturales (MNCN) - CSIC
C. de José Gutiérrez Abascal, 2, 28006 Madrid, Spain

Tuteur : Gerardo Benito
Fonction : Researcher / Professor

Léa Mesnil
IMA
2023-2024

Tuteur académique :
Stéphane Rodrigues

Acknowledgments

I am very grateful to have had the opportunity to do my internship in the Hydrology and Climate Change Laboratory. I would like to thank my supervisor Dr. Benito and Dr. Vázquez-Tarrío for their advice and support.

I want also to thank them and all the members of the laboratory, Mapi, Ishel, Paula, Jaime, Joe, Alberto, Ernesto, Tamir, Juan, and Jacek for their welcome and their kindness.

Contents

List of figures

List of tables

List of annexes

1. Introduction

This report presents my end-of-studies internship, part of the Aquatic Environment Engineering course in the Planning and Environment Department of the Engineering School Polytech Tours. It took place at the Museo de Ciencias Naturales, in the Geology Department, in Madrid, Spain from 8 April 2024 to 30 August 2024.

The internship is entitled "*Analysis of morpho-sedimentary dynamics of Mediterranean streams affected by human disturbance*". This internship suited me perfectly because I wanted to work on hydromorphology, and sedimentology issues and I am also really interested in hydraulic modelling. The objectives of this internship are:

- Analysis of the hydraulics conditions driving depositional and erosional landforms during flood events.
- Estimation of sediment transport rates based on empirical and field monitoring data.
- Assessment of hydromorphological adjustment and recovery potential of rivers following anthropogenic disturbance.

The research work has focused on an ephemeral Mediterranean stream named Rambla de la Viuda. The main objectives of it are to assess the trajectory of ephemeral streams over time and to gain a better understanding of morphosedimentary functioning, to anticipate the evolution of these rivers, which are subject to various pressures, in a context of global change.

The internship will therefore include data treatment with geomorphological mapping, Digital Terrain Models (DTM) and the generation of a suitable mesh for two-dimensional hydraulic modelling, data analysis with hydraulic/morpho-dynamics modelling based on before and after flood DTMs, and data interpretation.

2. Host structure presentation

2.1. Host organisation : Museo Nacional de Ciencias Naturales

The host organisation of the internship is the Museo Nacional de Ciencias Naturales (MNCN), situated in Madrid, which belongs to the Consejo Superior de Investigaciones Científicas. Regarding its history, it was founded in 1771 and is one of the most ancient Natural History Museums in the world (Museo Nacional de Ciencias Naturales, w. d.). The MNCN is structured into six research departments:

- Biodiversity and Evolutionary Biology.
- Biogeography and Global Change.
- Biogeochemistry and Microbial Ecology.
- Evolutionary Ecology.
- Geology.
- Paleobiology.

The Museo Nacional de Ciencias Naturales is open to the public and has eleven million specimens in its collections, attracting three hundred thousand visitors a year. Three hundred people including eighty researchers, work here and there are two hundred scientific projects per year (Museo Nacional de Ciencias Naturales, w. d.).

Figure 1: Museum organisation chart (Source: Museo Nacional de Ciencias Naturales)

2.2. Department of Geology

The Department of Geology studies the Earth's physical systems at different spatial and temporal scales (Museo Nacional de Ciencias Naturales, w. d.). That includes the causes and potential consequences of the Earth's natural processes such as floods, sea level changes, climate change or carbon cycle. The department also focuses on genesis, availability, distribution, and possible depletion of natural resources like soil pollution, water, minerals and rocks. (Museo Nacional de Ciencias Naturales, w. d.).

The internship project was specifically hosted at the Hydrology and Climate Change Laboratory with extensive experience in flood hydrology, historical hydrology, and natural hazards in mountain environments (Hydrology and Climate Change Laboratory, w. d.).

3. Missions and issues approached

3.1. Main mission

3.1.1. Context, objectives and study concerns

Intermittent rivers and ephemeral streams (IRES) are characterised by seasonal flows, the former during wet seasons and the later after heavy precipitation events. Currently, IRES account for more than 50% of the total length of the global river network (Skoulikidis et al., 2017), and comprises a large portion of Mediterranean watersheds. This list of IRES is expected to increase in the near future, since a suite of perennial rivers are extending their seasonal dryness due to climate change, land-use changes and water demands (Gallart et al., 2012).

It is a fact that the conservation of hydromorphological and fluvial habitats aspects in ephemeral streams has been largely ignored within the political and institutional contexts. This is partly due to the 'apparent' scarce economic interest given that they are not considered to hold the status of water bodies. The lack of flow favours human disturbance during the dry phases such as gravel mining, road traffic, conduits, dumping of trash and agricultural schemes (Gómez et al., 2005). In fact, the implementation of the European Water Framework Directive (WFD; Directive 2000/60/EU) has been optionally applied to ephemeral streams by watershed authorities at regional level in Mediterranean countries. Many of the Mediterranean ephemeral streams have been affected by gravel mining with important problems of their hydromorphological conditions, namely sediment depletion and sediment connectivity. Therefore, the study of sediment transport and morphodynamic changes during flow events it is a significant issue for ephemeral river recovery. Furthermore, knowing the sediment flow of a stream, as well as its transport capacity, can help predict geomorphic changes and potential erosion of a stream due to a lack of sediment supply.

The main objective of this internship project is to model morphodynamic changes and sediment flow during flood events. For this aim, the 2D HEC-RAS model (Hydrologic Engineering Center's River Analysis System) was selected because of its widely use, being a free software and for reliable capabilities for sediment transport modelling. The study was carried out in the Rambla de la Viuda, where hydrological data and field monitoring specifically Digital Terrain Models are available.

3.1.2. Presentation of the study site

The study site is the Rambla de la Viuda, a Mediterranean ephemeral stream located on the east of Spain, near Castellón de la Plana (Figure 2). This 76.40km-long river is mainly composed of gravels and drains a catchment area of 1524 km² (Figure 3 and 4).

The hydrology of this stream is influenced by its Mediterranean climate with hot dry summers and mild wet winters. Annual precipitation ranges between 400 mm close to the sea and about 700 mm at the headwaters. Most of the flow occurs during autumn and spring in relation to heavy rainfalls resulting from mesoscale convective systems (Camarasa and Segura, 2001).

Figure 2: Location of the Rambla de la Viuda (Source: L. Mesnil, 2024)

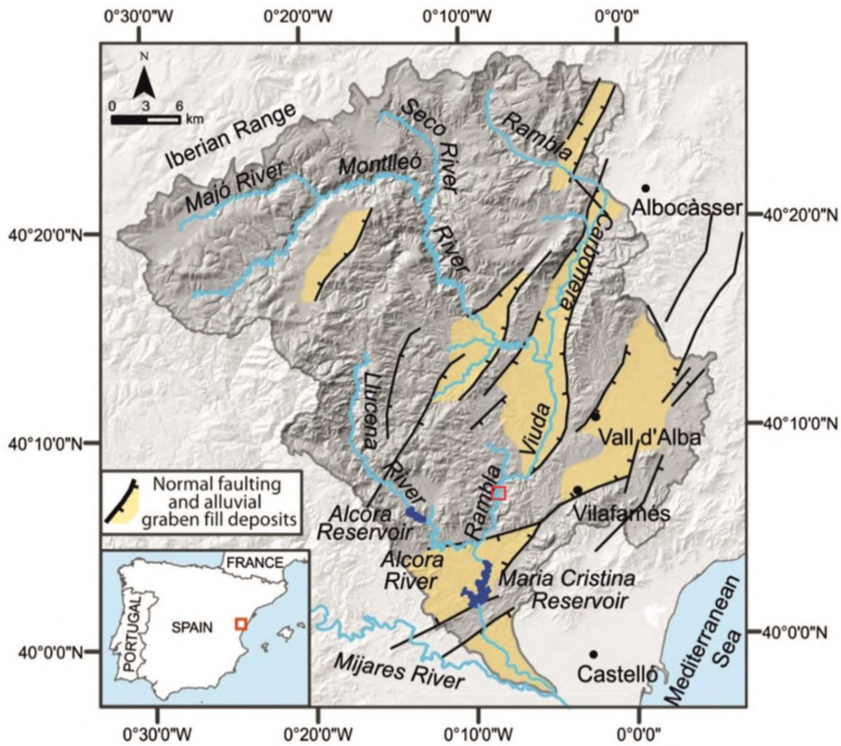

Figure 3: Location of the study site. The red square in the Rambla de la Viuda catchment shows the position of the modelled site (Source: Rabanaque et al., 2022)

Figure 4: Photographs of the Rambla de la Viuda near the junction with the Carretera de Vilafamés a Costur.

3.2. Different missions and associated issues

3.2.1. Rating curve determination

Real-time water depth was obtained using pressure transducers (PT), specifically a Levelogger® Edge Model 3001 manufactured by Solinst. The depth measurements were established with a time interval of 5 minutes. The device is located in the central-upstream part of the road crossing the stream. The atmospheric pressure correction to obtain the actual water depth was performed by a barologger located nearby of the pressure sensor.

The water discharge associated with the water depth from the sensor was obtained from a rating curve. The rating curve will allow to have a hydrograph for each flood event.

3.2.2. Estimation of the particle size distribution of the surface and subsurface layers

The grain-size distribution (GSD) of the surface riverbed sediment was determined based on samples taken using the Wolman method (Wolman, 1954). The data sampling from different landform units was carried out during a field survey in June 2015. The subsurface layer was estimated from empirical relationships of the upper layer particle size distribution.

The grain size distributions were associated to different landform units along the reach, meaning that a geomorphological map is critical for this purpose. Afterwards, it will allow to match the different land units with a grain size distribution and describe precisely the granulometry of the reach.

3.2.3. Determination of sediment flow

One of the main objectives was to determine the sediment flow in the Rambla de la Viuda, using 2D HEC-RAS modelling. The idea was to model one flood peak and compare the results with the observed field data. To achieve this, the data collected in the field was analysed, and the model was calibrated. The calibration entails optimising the mesh, choosing the computation time parameters, determining the appropriate boundaries conditions, and selecting the transport and hiding functions.

4. Methodology

4.1. Tasks entrusted

The tasks I was given involved running the hydraulic and sedimentary models on HEC-RAS. The first task was to establish the rating curve, then to start with the 2D modelling on HEC-RAS, primary hydraulically, and later with the sediment transport module. At the same time, I was able to estimate the particle size distribution of the surface and subsurface gravel bed layers. That allowed to improve my skills on HEC-RAS 2D modelling and enabled to expand my knowledge of sediment transport. I was helped and supported in these tasks by my tutor and Dr. Vázquez-Tarrío.

The Figure 5 presents the different tasks and components constituting the methodology followed.

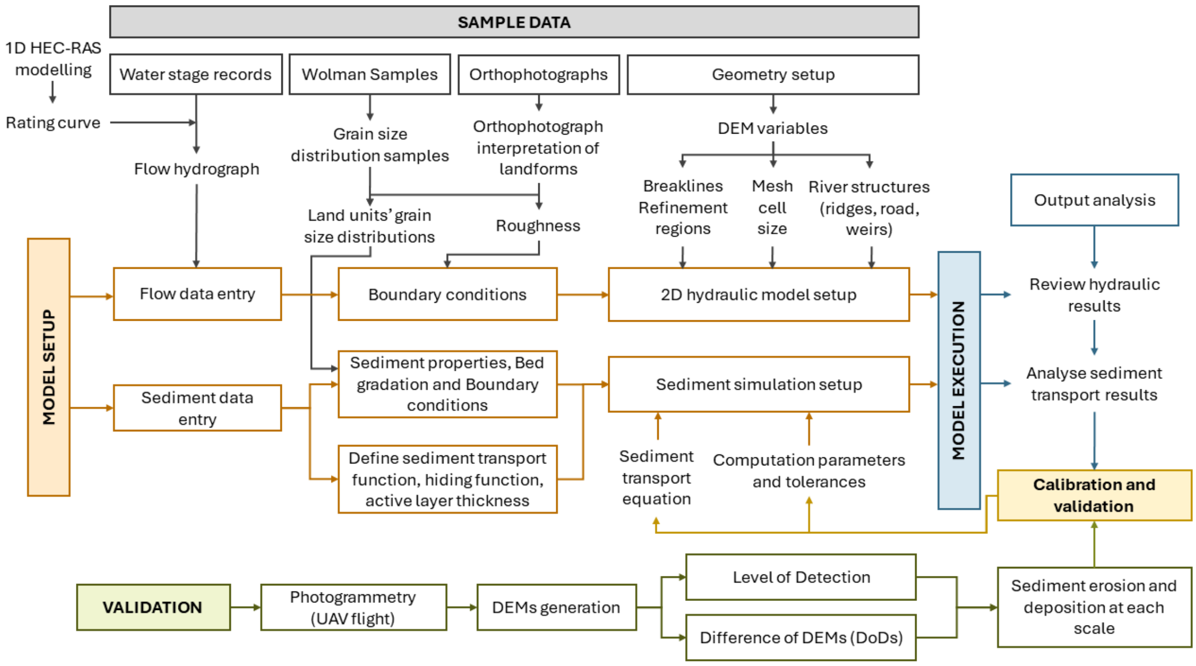

Figure 5: Methodology chart

4.2. General parameters to be set in HEC-RAS

4.2.1. Topography and computation time parameters

First of all, a modelling in HEC-RAS requires information about the topography and bathymetry of the modelled area. This way, the DTM of 2019 was specified.

Then, one of the parameters to be set in each calculation is the computation time-step. In HEC-RAS, it is possible to specify either a fixed time step, or a variable time step. In the first trial, the fixed time step is not advisable, because the computation may be stopped due to the error message "2D solution went unstable". For this reason, the time step was set to a variable time step, based on the Courant Number (Figure 6). The Courant Number corresponds to "a dimensionless measure, of the distance over which a constituent is advected through the computational grid." (HEC-RAS Water Quality Technical Reference, 2018). Once the computation time is obtained based on Courant, it can be used to fix the computation time for the following runs.

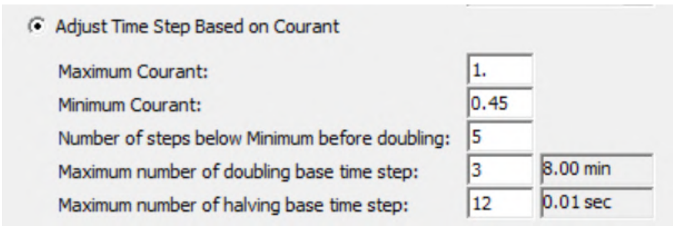

Figure 6: Time step parameters

4.2.2. Mesh selection and optimisation

In order to carry out 2D modelling with HEC-RAS, it is necessary to create a mesh that the software uses for its calculations. The mesh is made of polygons, often squares, but sometimes with more sides when breaklines are introduced.

To construct a mesh, a perimeter has to be specified. The perimeter consists of a polygon that surrounds the area to be modelled. After defining the width of the cells, the mesh can be generated within this boundary. The accuracy of the mesh can also be refined using the “breaklines” or “refinement regions” tools.

Several calculations were carried out with a different cell size for the mesh defined within perimeter of the study area. The cell sizes tested were 3x3 metres, 5x5 metres and 10x10 metres. The cell size is a compromise between the precision of the results, particularly for the bed change, which provides a single value per cell, and the duration of the computation. It emerged that even for a mesh of 5x5 metres cells, the duration of the computation is much longer than for a mesh of 10 x 10 metres cells. It is also important to note that these are simple calculations, and the addition of sediment data will further increase the computation time. For this reason, the final cell size was set at 10x10 metres.

In the study area, the main areas to be improved are the banks and the river channel next to the road, which represents an abrupt change in height upstream and downstream it. Then the next question was what tool could be used to improve these areas. According to the literature, breaklines can accurately defined the banks of the reach and the brutal changes of elevation (Stanford, 2021). Moreover, the breaklines can also be used to orientate the cells of the mesh perpendicularly to the flow (Stanford, 2021).

During the initial model computations, some gaps appeared in the results, located on the road, that fit into certain cells of the mesh (Figure 7). To correct these problems, the breaklines were slightly adjusted and several iterations were run to control the effectiveness of the corrections. Finally, the geometry presented in Annexe 6 was obtained.

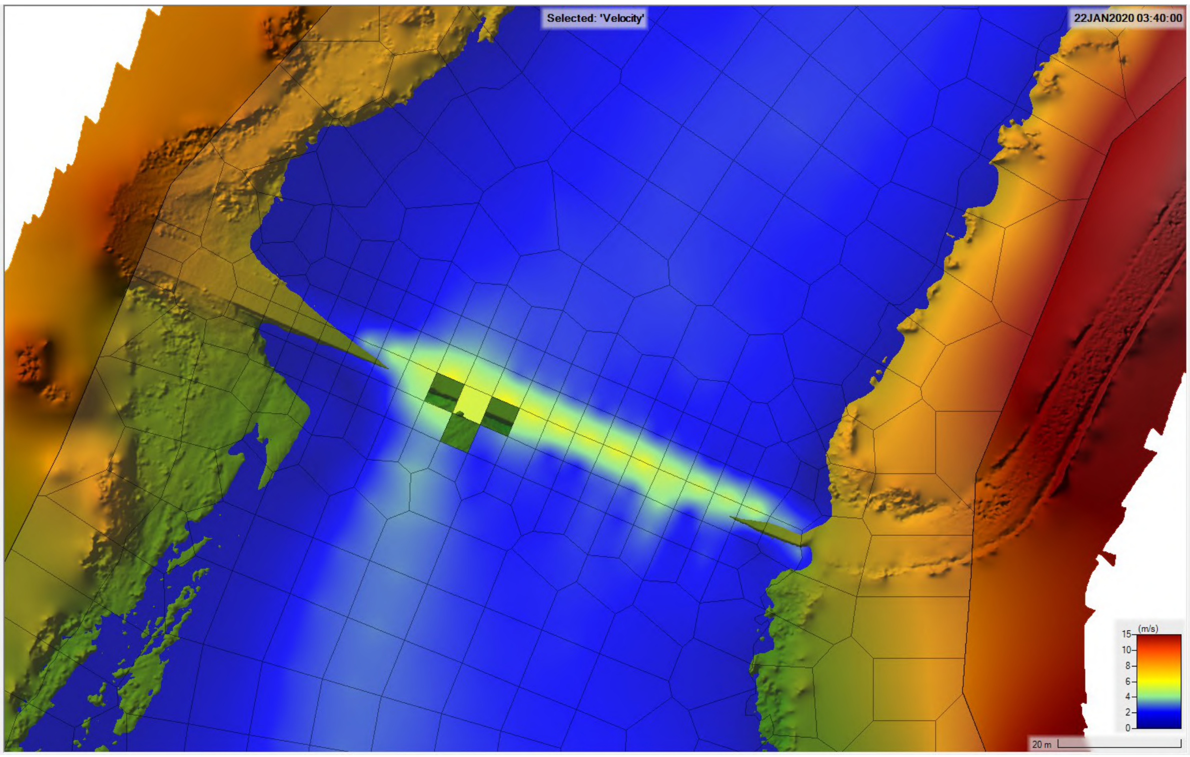

Figure 7: Holes in the velocity results

4.3. 2D hydraulic Modelling

4.3.1. Land units and Manning's n values

The spatial distribution of hydraulic parameters of the study area (e.g. roughness, grain size) are associated with the landform units, classified in terms their morphosedimentary and vegetation cover characteristics. For instance, the roughness is directly affected by the presence of vegetation, its density and composition (trees, bushes etc.), also by the surface grain-size and soil cover (boulder, bedrock or asphalt). In modelling software, the roughness parameter can be introduced in the model by specifying the Manning or Strickler's coefficient, knowing that the Strickler's value is 1 / Manning's value. In our case, the Manning's values were introduced to HEC-RAS. For this purpose, a land unit map has been produced, so each landform can be assigned to a Manning's value.

A first stage previous to the mapping of the land units involves the construction of a legend. This allows to categorise and describe the main landform units. Table 1 lists the land unit classes and a basic description of their characteristics. The Manning's n values were assigned to each land unit based on the soil cover and the density of the vegetation. For instance, an area with a strong vegetation density has a Manning's value higher than an unvegetated area. The values were estimated based on the Table of Chow (1959), available in this website.

Table 1: Type and description of land units and associated Manning's n values

Land unit	Description	Manning's values
Channel low flow	Water channel with low flow rate	0.025
Channel high flow	Water channel with high flow rate	0.028
Unvegetated lateral bar	Lateral bar without vegetation	0.028
Barely vegetated lateral bar	Lateral bar covered by grasses and scattered shrubs (25%)	0.028/0.035
Mixed vegetated lateral bar	Lateral bar covered by shrubs (<50%) and scattered trees (25%)	0.045
Unvegetated median bar	Median bar without vegetation	0.028
Barely vegetated median bar	Median bar covered by grasses and scattered shrubs (25%)	0.028
Mixed vegetated median bar	Median bar covered by shrubs (<50%) and scattered trees (<5%)	0.045
Lobes	Fresh fine to medium gravel deposited on channel low flow areas	0.028/0.035
Fully vegetated area (slope)	Area covered by shrubs (75%) and scattered trees (<25%)	0.07
Tree covered alluvial area	Area covered by compact masses of trees in alluvial areas	0.1
Bed rock exposure	Bedrock outcrops mainly limestone and conglomerates	0.04
Colluvium	Colluvium with dense vegetation	0.25

Several types of data were used to produce the land unit map, namely Digital Terrain Model (DTM), and orthophotographs. The DTM was obtained using photogrammetry from aerial photographs taken on the field from an UAV (Drone flight). The UAV flight was performed in June 2019, and its precision is in the range of five centimetres. The orthophotographs were supplied from the Generalitat Valenciana web page.

In fact, the orthophotographs were slightly modified to accentuate some colours. For instance, the colour green that represents the trees are important information when constructing a land unit map, since the classification in each type of land unit was supported by the vegetation density as an age indicator. The green colour has been modified into a red colour, to get more contrast with the gravels, which appear more white or grey (Annexe 1). Regarding the DTM, it was duplicated into two layers to use two different representations. The first one was the common terrain model product, with a gradation of colours, and the second one corresponds to a hill-shade map (Annexe 2 and Annexe 3).

The land units were subdivided on the basis of the criteria described above in Table 1. The density of the vegetation was an important element on which we have based the land unit mapping. Other criteria were the slope breaks limiting the unit and the elevation in relation to the river thalweg observed on the DTM. Then, from upstream to downstream of the study area, the land units where gradually identified (Annexe 4). It was sometimes difficult to divide certain areas, which appeared to contain several geomorphological entities, because the boundaries were not always evident.

Once the map was completed, Manning's values were assigned to each type of land unit. The minimum Manning's value was assigned to the concrete road (0.015) and the maximum to the colluvium (0.25) (Annexe 5). Then, in HEC-RAS, a land cover layer was created consisting of a layer with different land units and their associated Manning's n values.

4.3.2. Rating curve

The data available for the hydrological input are the water surface elevations recorded at 5-minute intervals in sensors located on the edge of the road crossing the stream. The transformation from the water surface elevations (depth) to water discharges requires the creation of a rating curve at the sensor site. The 1D HEC-RAS software was selected due to its ease of use.

The 1D HEC-RAS data entry requests multiple cross-sections with precise elevation values. Here, these cross-sections upstream and downstream of the road were input from field data obtained with a high precision GPS GNSS (Trimble R12).

First of all, the cross-sections obtained in the field have been modified before being used in the HEC-RAS model. The points taken in the field were displayed on ArcGIS. A line between all the points of one cross-section was drawn which enabled to check if the points follow a straight line and that if lines were perpendicular to the flow, as this is important issue on 1D HEC-RAS modelling. If necessary, the lines have been redrawn to be more perpendicular and the points were translated to these lines. Then the coordinates (X, Y) of each point were calculated with ArcGIS. Because they were not moved far from their original position, it was assumed that their elevation (Z) was the same.

In total, five cross-sections were taken on the field: two on the road, and three upstream of the road. To make the model more representative, additional cross-sections were added based on the DTM of June 2020. For this purpose, it was checked that the point elevations on the road from the DTM closely matched those from the field GPS cross-sections. The coordinate values of these new cross-sections were extracted from the DTM and exported to a table. However, HEC-RAS can only use 500 values per cross-section, while the cross-sections from the DTM have approximately 1500 values. Therefore, some of the values were deleted. To achieve this, each point was assigned to a label (a, b or c), depending on the number of points to be removed, and only the points corresponding to one label were kept.

A 1D modelling was then run on HEC-RAS using critical depth for upstream and downstream boundary conditions. Fifty flow values were entered into the model to describe the rating curve. After running the model, various hydraulic parameters were obtained for each cross-section, including water surface elevation, channel velocity and Froude number. To obtain the rating curve, the cross-section of the road where the level sensor is located, the one of the downstream side, was selected because the Froude number was equal to 1, indicating critical flow.

The Excel function "LINEST" was then used to accurately determine the coefficients of the polynomial trendline function, with an equation of the form $ax^2 + bx + c$ (Figure 8). Once these coefficients were known (Table 2), this polynomial function was applied to the water surfaces elevation values to obtain the rating curve. Finally, the water surface elevation recorded in the sensor level during the January 2020 flood were used to obtain the flow rates using the rating curve (Figure 9).

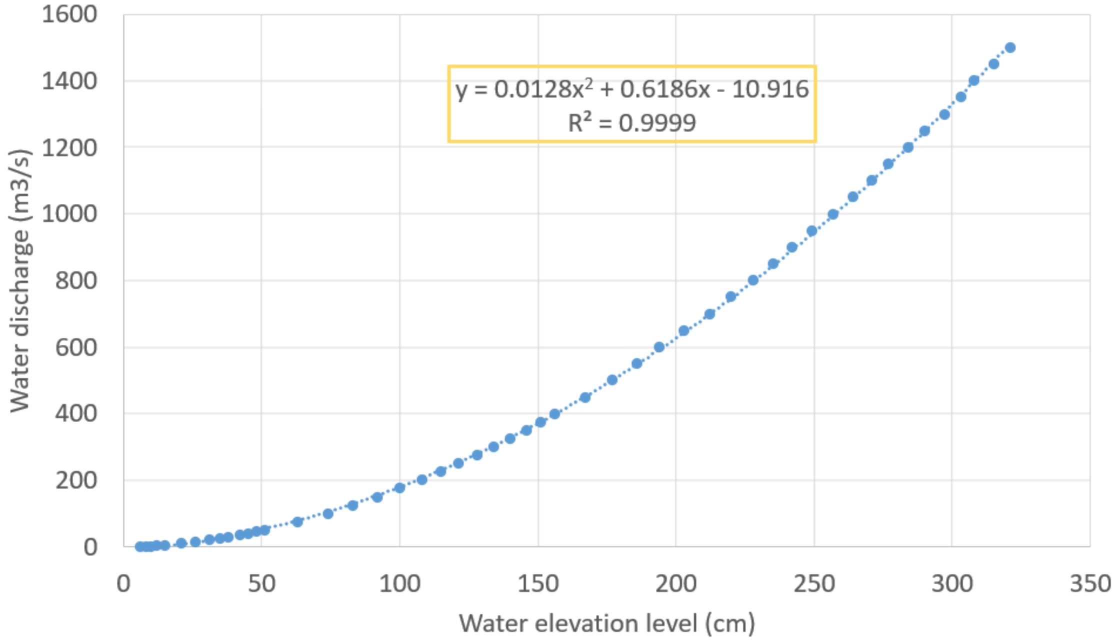

Figure 8: Rating curve graphical representation (Source: L. Mesnil, 2024)

Table 2: Rating curve coefficients

a	b	c
0.01284284	0.61855898	-10.915791

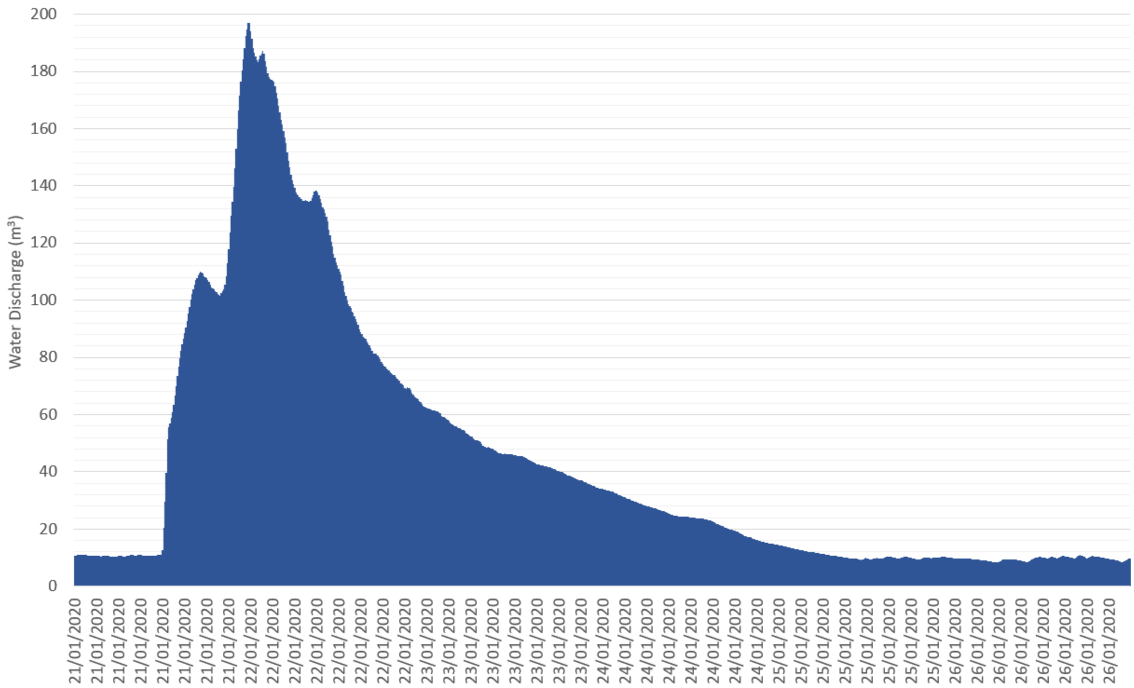

Figure 9: Hydrograph obtained with the rating curve (Source: L. Mesnil, 2024)

4.3.3. Boundary conditions

Once the mesh geometry has been completed, and the hydrograph computed, the boundary conditions upstream and downstream of the reach must be specified. It is possible to enter different boundary conditions, namely:

- Stage Hydrograph
- Flow Hydrograph
- Normal Depth
- Rating Curve

In our modelling the flow hydrograph has been used for the upstream boundary conditions, whereas the normal depth has been selected as the downstream boundary condition. To indicate the Flow Hydrograph, it is necessary to specify the flow rate according to a pre-selected time step and to enter the parameter "EG Slope for distributing flow along BC Line". This parameter can be calculated from the DTM by taking the slope along the boundary condition line. In our case it is equal to 0.017 m/m. The flow rates used were computed using the rating curve and the water surface elevation during a flood peak in January 2020. The hydrograph lasted approximately five days from 21 January 2020 to 25 January 2020. To know the Normal Depth, the slope parallel to the flow was calculated from the 2019 DTM, in the last downstream part of the reach, and is 0.006 m/m.

4.4. 2D morpho-dynamics modelling

4.4.1. GSD data

In gravel-bed rivers, sediment transport involves the movement of both surface and subsurface sediment layers. These layers have distinct characteristics and play different roles in the transport processes that can be modelled by HEC-RAS. The sediment characterisation requires field surveys and statistical analysis of the gravel grain sizes. The GSD was obtained from field surveys along the stream carried out in 2015. For each sample, one hundred particles were collected using the Wolman method. In this case, two 25-metre measuring tapes were laid parallel on the ground of the gravel unit to be characterised, and a particle was pick-up along the tape every 0.5 m. Using the Wolman grid, the value of the b-axis of the sediment was recorded in a table per class. In total there were fifty-eight samples.

4.4.2. Estimation of the GSD of the upper layer

The surface layer, often referred to as the "armour layer," consists of larger, coarser particles. This layer is typically more stable and resistant to movement compared to the subsurface layer. The particle size distribution of the surface layer area was associated with each land unit for their integration into HEC-RAS model. Some of the samples from the Wolman field surveys were located exactly on some of the land units of the study reach. In these cases, if several samples were present on the same type of land unit, the sample with the average granulometric distribution was chosen. Conversely, if there was no sample located on one of the land units of the studied reach, a granulometry sample from an equivalent land unit outside of the study area was selected.

The values of each sample were then adjusted to the classes requested by HEC-RAS. Most of the original grain-size class intervals fit with those required by HEC-RAS (Table 3). In the case that the HEC-RAS classes corresponded to two original field classes, the two values of the sample with original classes were added to obtain the value for the new classes (Figure 10). When the original classes corresponded exactly to those of HEC-RAS, the values were simply taken as they were.

To obtain the grain size distribution, the cumulative increasing numbers were calculated from the samples values per class adapted to the HEC-RAS's requirements, and the percentage per class was calculated (Figure 10).

Table 3: Original field classes (left) and classes required by HEC-RAS (right)

Original field classes (mm)
< 2
2
2.8
4
5.6
8
11
16
22.6
32
45
64
90
128
180
256
512

HEC-RAS classes (mm)
0.004
0.008
0.016
0.032
0.0625
0.125
0.25
0.5
1
2
4
8
16
32
64
128
256
512
1024
2048

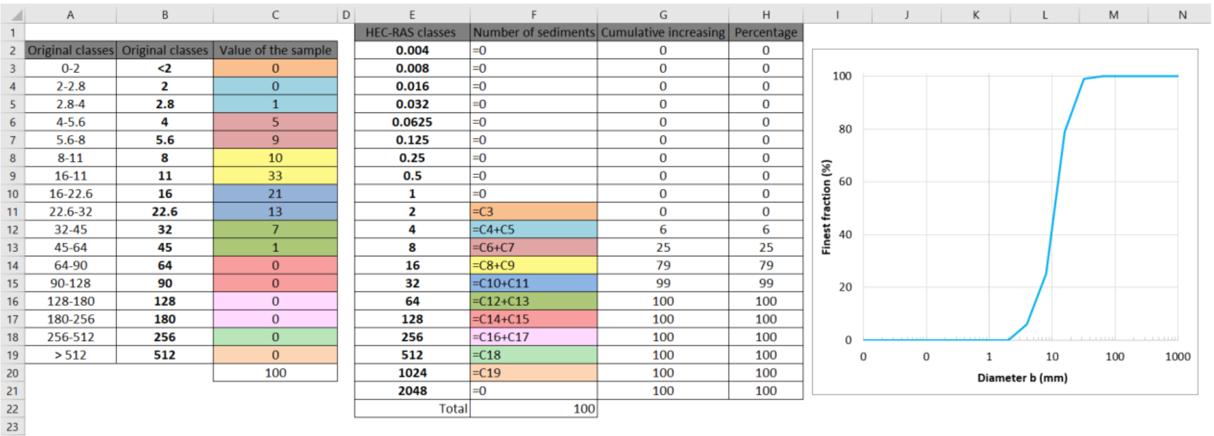

Original classes	Original classes	Value of the sample
0-2	<2	0
2-2.8	2	0
2.8-4	2.8	1
4-5.6	4	5
5.6-8	5.6	9
8-11	8	10
16-11	11	33
16-22.6	16	21
22.6-32	22.6	13
32-45	32	7
45-64	45	1
64-90	64	0
90-128	90	0
128-180	128	0
180-256	180	0
256-512	256	0
> 512	512	0
		100

HEC-RAS classes	Number of sediments	Cumulative increasing	Percentage
0.004	=0	0	0
0.008	=0	0	0
0.016	=0	0	0
0.032	=0	0	0
0.0625	=0	0	0
0.125	=0	0	0
0.25	=0	0	0
0.5	=0	0	0
1	=0	0	0
2	=C3	0	0
4	=C4+C5	6	6
8	=C6+C7	25	25
16	=C8+C9	79	79
32	=C10+C11	99	99
64	=C12+C13	100	100
128	=C14+C15	100	100
256	=C16+C17	100	100
512	=C18	100	100
1024	=C19	100	100
2048	=0	100	100
Total	100		

Figure 10: Conversion between original field classes and HEC-RAS classes (Source: L. Mesnil, 2024)

4.4.3. Calculation method for the GSD of the subsurface layer

After having introduced variability in the sediment distribution along the reach in a horizontal dimension (surface), the texture composition in the vertical axis (subsurface) was also entered (Figure 11). Subsurface GSD is usually determined based on bulk volumetric samples (Bunte and Abt, 2001). However, collecting volumetric samples is a time-consuming task that requires large sample volumes, often over 100 kilograms, in gravel-bed streams to be representative (Church et al., 1987). The large geographical distance between the Rambla de la Viuda and MNCN did not facilitate this task. For these reasons, no volumetric samples of subaqueous sediment were collected in the study reach for this work. Thereby, the sediment size distribution has been calculated for the subsurface layer, based on Recking's (2017) empirical model, which is based on a large database of GSD from gravel-bed rivers.

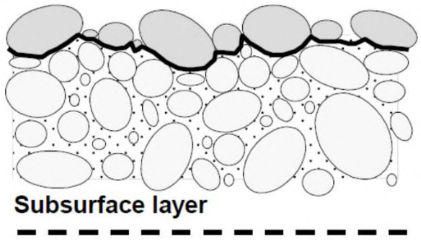

Figure 11: Surface and subsurface sediment layers within a riverbed (Source: Bizzi et al., 2014)

To do that, the method used needs the D_{50} and D_{84} values (Recking, 2017). We assumed an armour ratio that is approximately equal to 1.5, which based on the systematic review done by Vázquez-Tarrío et al. (2020). It is a value expectable for rivers similar to the Rambla de la Viuda. Regarding the D_{50} from the subsurface layer, we therefore assumed that it equals the D_{50} of the surface layer divided by 1.5. The D_{84} of the subsurface was considered equal to the D_{84} of the surface layer (Vázquez-Tarrío et al., 2020) (Table 4). For the Fs fraction, we assumed that it was 15% of the grain size distribution of the subsurface layer (Vázquez-Tarrío et al., 2020). As the surface granulometric distribution does not contain a Fs fraction, the minimum diameter fraction was considered to be equal to 15%. The grain size distribution for the subsurface layer was then estimated using the general empirical relationships used to calculate a grain size distribution, shown in Table 5 (Recking, 2017).

Table 4: D50 and D84 values for the surface and subsurface

Sample	Land unit	D_{50} surface (mm)	D_{84} surface (mm)	D_{min} (mm)	D_{50} subsurface (mm)	D_{84} subsurface (mm)
AF1	Mixed vegetated lateral bar	27.71	53.65	8	18.47	53.65
AF12	Channel high flow	15.00	27.32	4	10.00	27.32
AF42	Lobes	42.32	93.71	8	28.22	93.71
AF46	Unvegetated median bar	14.49	28.34	4	9.66	28.34
AF49	Barely vegetated median bar	39.38	76.80	16	26.26	76.80
AF54	Barely vegetated lateral bar	20.29	41.85	4	13.53	41.85
AF56	Unvegetated lateral bar	23.11	38.74	8	15.41	38.74
AF57	Channel low flow	31.47	74.11	2	20.98	74.11

Table 5: General method for estimating grain size distribution (Source: Recking, 2017)

Class	*i* (%)	D_i (mm)	C_n
1	$100F_s$	D_{min} (≥2mm)	-
2			16
3	$\frac{50-100F_s}{C_n}+100F_s$	$\frac{D_{50}-D_{min}}{C_n}+D_{min}$	3.3
4			1.9
5			1.3
6	50	D_{50}	-
7	60	$\frac{D_{84}-D_{50}}{C_n}+D_{50}$	5.9
8	70		2.3
9	84	D_{84}	-
10	90		1.3
11	98	$C_n D_{84}$	2.5
12	100		5.1

Once the subsurface layer GSDs have been obtained, the results must be adjusted to HEC-RAS classes. In other words, the limits of the intervals in Table 5 depend on the D_{50}, D_{84} and the C_n coefficient and do not necessarily correspond to those of HEC-RAS. This was done by interpolating to find the finest percentage for the limit of each interval (Figure 12). Finally, the vertical GSDs were entered into HEC-RAS, within three main layers: (1) a surface amour layer of 15 centimetres in thickness, (2) a subsurface layer of 1 metre in thickness, and (3) a non-erodible surface of 2 metres in thickness.

	A	B	C	D	E	F	G
1							
2		Sample AF1 subsurface Layer				Sample AF1 subsurface Layer	
3		Diameter (mm)	Finest percentage		HEC-RAS class (mm)	Finest percentage	Finest percentage
4		8.00	15.00		0.004	0.00	0.00
5		8.65	17.19		0.008	0.00	0.00
6		11.17	25.61		0.016	0.00	0.00
7		13.51	33.42		0.032	0.00	0.00
8		16.06	41.92		0.0625	0.00	0.00
9		18.47	50.00		0.125	0.00	0.00
10		24.43	60.00		0.25	0.00	0.00
11		33.77	70.00		0.5	0.00	0.00
12		53.65	84.00		1	0.00	0.00
13		69.74	90.00		2	0.00	0.00
14		134.12	98.00		4	0.00	0.00
15		273.60	100.00		8	=C4	15.00
16					16	=C7+(E16-B7)/(B8-B7)*(C8-C7)	41.74
17					32	=C10+(E17-B10)/(B11-B10)*(C11-C10)	68.11
18					64	=C12+(E18-B12)/(B13-B12)*(C13-C12)	87.86
19					128	=C13+(E19-B13)/(B14-B13)*(C14-C13)	97.24
20					256	=C14+(E20-B14)/(B15-B14)*(C15-C14)	99.75
21					512	100.00	100.00
22					1024	100.00	100.00
23					2048	100.00	100.00

Figure 12: Interpolations to obtain the finest percentage the HEC-RAS for the grain size distribution classes of the subsurface layer (Source: L. Mesnil, 2024)

4.4.4. Sediment boundary condition and computation time parameters

In the HEC-RAS model, a "warm-up" period is a crucial component, especially in unsteady flow simulations. This ensures the model to stabilise before the main simulation period begins. In the computations made, the warm-up lasted 24 hours. It is important because usually at the beginning of a model running, the reach is dry, thus it could lead to inconsistencies in the model results if a sediment layer is added without warm-up.

Moreover, in a 2D sedimentary modelling, a boundary condition needs to be specified such as the upstream sediment flux (load). Note that these sediment data are independent of the sediment gradations from the riverbed introduced previously, which corresponds to the surface and subsurface layers grain size distributions.

HEC-RAS allows to specify the upstream sediment boundary condition, which can be:

- Rating Curve
- Sediment Load Series
- Equilibrium Load
- Capacity Ratio
- Clear Water (No sediment)

Prior to run the definitive model, some previous tests were made to analyse the sensitivity of model outcomes to different model parameters. For some of these runs, the Capacity Ratio boundary condition was used, while in others the Sediment Load Series was used.

In the case of the Sediment Load Series boundary condition, it is necessary to enter the amount of sediment in tons per time-step, which can be modified. Moreover, it is required to provide a gradation rating curve of sediment amounts, in ton per day. To define this rating curve, a subsurface grain size distribution was taken, as this distribution corresponds more closely to the bedload than the surface one. The percentage value of each class was multiplied by 0.00001 and by 10000000, to have the rating curve. An average subsurface layer sample was used to obtain the sediment rating curve (Figure 13).

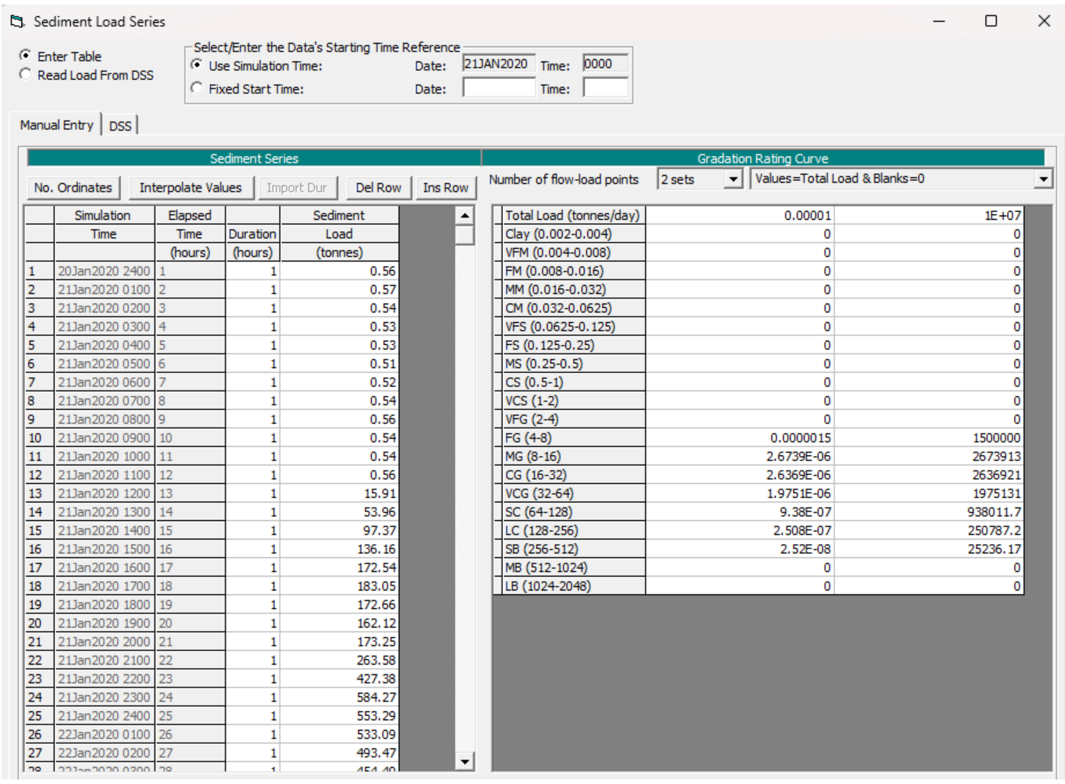

Sediment Load Series

Enter Table / Read Load From DSS

Select/Enter the Data's Starting Time Reference: Use Simulation Time: Date: 21JAN2020 Time: 0000; Fixed Start Time: Date: Time:

Manual Entry | DSS

Sediment Series

No. Ordinates | Interpolate Values | Import Dur | Del Row | Ins Row

	Simulation Time	Elapsed Time (hours)	Duration (hours)	Sediment Load (tonnes)
1	20Jan2020 2400	1	1	0.56
2	21Jan2020 0100	2	1	0.57
3	21Jan2020 0200	3	1	0.54
4	21Jan2020 0300	4	1	0.53
5	21Jan2020 0400	5	1	0.53
6	21Jan2020 0500	6	1	0.51
7	21Jan2020 0600	7	1	0.52
8	21Jan2020 0700	8	1	0.54
9	21Jan2020 0800	9	1	0.56
10	21Jan2020 0900	10	1	0.54
11	21Jan2020 1000	11	1	0.54
12	21Jan2020 1100	12	1	0.56
13	21Jan2020 1200	13	1	15.91
14	21Jan2020 1300	14	1	53.96
15	21Jan2020 1400	15	1	97.37
16	21Jan2020 1500	16	1	136.16
17	21Jan2020 1600	17	1	172.54
18	21Jan2020 1700	18	1	183.05
19	21Jan2020 1800	19	1	172.66
20	21Jan2020 1900	20	1	162.12
21	21Jan2020 2000	21	1	173.25
22	21Jan2020 2100	22	1	263.58
23	21Jan2020 2200	23	1	427.38
24	21Jan2020 2300	24	1	584.27
25	21Jan2020 2400	25	1	553.29
26	22Jan2020 0100	26	1	533.09
27	22Jan2020 0200	27	1	493.47

Gradation Rating Curve

Number of flow-load points: 2 sets | Values=Total Load & Blanks=0

Total Load (tonnes/day)	0.00001	1E+07
Clay (0.002-0.004)	0	0
VFM (0.004-0.008)	0	0
FM (0.008-0.016)	0	0
MM (0.016-0.032)	0	0
CM (0.032-0.0625)	0	0
VFS (0.0625-0.125)	0	0
FS (0.125-0.25)	0	0
MS (0.25-0.5)	0	0
CS (0.5-1)	0	0
VCS (1-2)	0	0
VFG (2-4)	0	0
FG (4-8)	0.0000015	1500000
MG (8-16)	2.6739E-06	2673913
CG (16-32)	2.6369E-06	2636921
VCG (32-64)	1.9751E-06	1975131
SC (64-128)	9.38E-07	938011.7
LC (128-256)	2.508E-07	250787.2
SB (256-512)	2.52E-08	25236.17
MB (512-1024)	0	0
LB (1024-2048)	0	0

Figure 13: Sediment Load Series input with the sediment graph (left) and the gradation rating curve (right)

The time-step for the sediment amount was set to one hour. To estimate the sedimentgraph, the Recking's (2017) sediment transport function was used. This function requests the Shields number which directly depends on the shear stress (Figures 14 and 15). The Shields parameter was calculated for diameter D_{84}.

$$\Phi = 14 \frac{\tau^{*2.5}}{1 + \left(\frac{\tau_m^*}{\tau^*}\right)^4}$$

Figure 14: Recking's equation, Dimensionless transport rate formula

$$\tau^* = \frac{\tau}{g(\rho_s - \rho)D}$$

$$\tau_m^* = (5S + 0.06)\left(\frac{D_{84}}{D_{50}}\right)^{4.4\sqrt{S}-1.5}$$

Where

$\tau =$ Shear stress [N/m^2]

$\tau^* =$ Shields parameter calculated for diameter D_X [ ]

$\tau_m^* =$ Mobility Shields stress [ ]

$S =$ Slope [m/m]

Figure 15: Shields parameters formulas

The shear stress values for applying Recking's equation were obtained by running 2D HEC-RAS modelling without sediment layer. Once the model has been run, shear stress values can be retrieved along a cross-section near the upstream boundary line, and this for several values of water discharges. Then, by computing the average shear stress value for the cross-section, it allows to get a rating curve giving a relationship between the shear stress and the water discharge. As done previously for the hydrograph, the coefficients of the trendline allowed computing the shear stress value for each flow rate.

Afterwards, the Recking's equation was applied to get the sediment graph by computing the dimensionless transport rate Φ. The volumetric bedload transport rate per unit width q_{sv} (Figure 16) was then computed, depending on Φ. This allowed to know the volumetric bedload transport rate by multiplying q_{sv} by the width and then by multiplying it by the sediment density, the sediment transport rate was obtained (Figure 17).

$$\Phi = \frac{q_{sv}}{\sqrt{g\left(\frac{\rho_s}{\rho} - 1\right) D^3}}$$

Where
$q_{sv} =$ Volumetric bedload transport rate per unit width $[m^3/m/s]$
$\rho_s =$ Sediment density $[kg/m^3]$
$\rho =$ Fluid density $[kg/m^3]$
$g =$ Intensity of graivty $[m/s^{-2}]$
$D_X =$ Grain diameter (subscript denotes % finner)[m]

Figure 16: Dimensionless transport rate and volumetric bedload transport rate per unit width formula

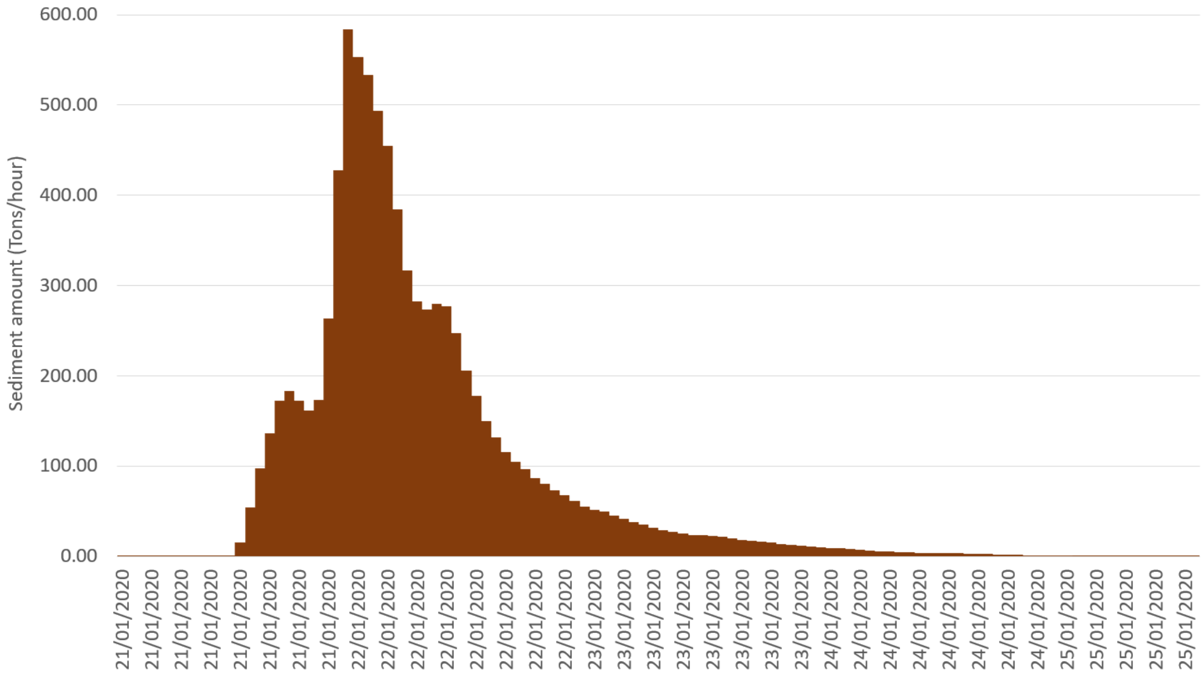

Figure 17: Estimated sedimentgraph (Source: L. Mesnil, 2024)

4.4.5. Transport functions, sorting and fall velocity methods

There are numerous parameters to be changed in the sediment modelling such as the transport function, the sorting method and the fall velocity method. In this study, the selected transport functions were the Meyer-Peter Müller and the Wilcock-Crowe ones (Figure 18 and 19).

$$\frac{q^*_{bk}}{\sqrt{R_k g d_k^3}} = A_M \rho_{sk} \left(\theta'_b - \theta_{crk}\right)^{E_M}$$

where
$\theta'_b = \frac{\tau'_b}{(\rho_{sk} - \rho_w) g d_k}$ = grain-related Shields parameter [-]
ρ_{sk} = sediment density [M/L^3]
ρ_w = water density [M/L^3]
θ_{crk} = critical Shields parameter [-]
A_M = empirical coefficient [-]

Figure 18: Meyer-Peter Müller formula used in HEC-RAS, with AM = 8, EM= 3/2 and ϑ_{crk} = 0.047 (Source: HEC-RAS 2D Sediment Technical Reference Manual, w. d.)

$$W_k^* = \begin{cases} 0.002\phi^{7.5} & \text{for } \phi < 1.35 \\ 14\left(1 - \frac{0.894}{\phi^{0.5}}\right)^{4.5} & \text{for } \phi \geq 1.35 \end{cases}$$

where

$\phi = \tau_b/\tau_{r,\ k}$ = sediment mobility [-]

τ_b = bed shear stress [-]

$\tau_{r,\ k}$ = reference shear stress

$$q_{bk}^* = \frac{u_*^3 W_k^*}{R_k g}$$

where

$q_{bk}{}^*$ = fractional bed-load sediment transport potential [L^2/T]

u_* = bed shear velocity [L/T]

W_k* = transport function [-]

$R_k = \rho_{sk}/\rho_w - 1$ = submerged specific gravity of grain class [-]

ρ_{sk} = sediment grain density [M/L^3]

ρ_w = water density [M/L^3]

g = gravitational constant [L/T^2]

Figure 19: Wilcock-Crowe formula used in HEC-RAS (Source: HEC-RAS 2D Sediment Technical Reference Manual, w. d.)

In addition to the transport equation, a hiding function was used in the modelling. When the Meyer-Peter Müller formula was selected, the hiding function chosen was Parker et al. with the hiding exponent equals to 0.77 (López et al., 2023). In the case of the Wilcock-Crowe formula, the hiding function was set to the Wilcock-Crowe hiding function by default (Figures 20 and 21).

$$\xi_k = \left(\frac{d_k}{d_{50}}\right)^{-m}$$

where m is an empirical coefficient between 0.5 to 1.0

d_k = grain size diameter [L]

Figure 20: Parker et al.'s hiding function (Source: HEC-RAS 2D Sediment Technical Reference Manual, w. d.)

$$\xi_k = \frac{\tau_{r,k}}{\tau_{r,sm}} = \left(\frac{d_k}{d_{sm}}\right)^{b_k}$$

where

$\tau_{r,\ k}$ = reference shear stress corresponding to d_k

$\tau_{r,m}$ = reference shear stress corresponding to d_m

d_k = grain size diameter [L]

d_{sm} = surface mean grain size diameter [L]

The empirical exponent b_k is given by $b_k = \dfrac{0.67}{1 + \exp\left(1.5 + \frac{d_k}{d_{sm}}\right)}$

Figure 21: Wilcock-Crowe's hiding function (Source: HEC-RAS 2D Sediment Technical Reference Manual, w. d.)

Finally, in every modelling, the fall velocity method was set to the Dietrich's equation (Figure 22) and the sorting method chosen was the Active Layer. Concerning the Active Layer, in the options, the thickness of it was X d90, with a multiplier equal to 4 (Vázquez-Tarrío et al., 2021) and the minimum Active Layer thickness has been set to 0.02 metres.

$$\frac{\omega_{sd}^3}{Rg\nu} = W_* = R_3 10^{R_1+R_2}$$

where

$R = \rho_s/\rho_w - 1$ = Submerged specific gravity [-]

ρ_s = particle density [M/L^3]

ρ_w = pater density [M/L^3]

g = gravitational constant (~9.81 m/s^2) [L/T^2]

$$R_1 = -3.76715 + 1.92944 \log_{10} D_* - 0.09815(\log_{10} D_*)^2 - 0.00575(\log_{10} D_*)^3 + 0.00056(\log_{10} D_*)^4$$

$$R_2 = \left[\log_{10}\left(1 - \frac{S_F}{0.85}\right)\right] - (1 - S_F)^{2.3} \tanh(\log_{10} D_* - 4.6) + 0.3(0.5 - S_F)(1 - S_F)^2(\log_{10} D_* - 4.6)$$

$$R_3 = \left\{0.65 - \left[\frac{S_F}{2.83}\tanh\left(\log_{10} D_* - 4.6\right)\right]\right\}^{1+(3.5-P)/2.5}$$

$$D_* = \frac{Rgd_n^3}{\nu^2}$$

ν = kinematic viscosity [L^2/T]

S_F = Corey (1949) shape factor (typically 0.6 - 0.7) [-]

P = Powers (1953) roundness index (typically 3.5) [-] (see also Folk 1955)

Figure 22: Dietrich's particle settling velocity method (Source: HEC-RAS 2D Sediment Technical Reference Manual, w. d.)

4.5. Model calibration

4.5.1. Sensitivity study of the model

As the morphodynamic model is sensitive to two parameters which are the sediment input and the sediment transport equation, the sensitivity study has focused on these two parameters.

In this way, eight models were run using the Capacity Ratio for the upstream boundary condition. Four of them were run with the Meyer-Peter Müller sediment function and the others with the Wilcock-Crowe sediment function. For each set of four model's runs, four different values of Capacity Ratio were used: 0, 0.25, 0.5 and 1. Then, the model was run using the Sediment Load Series sediment boundary condition, using the Wilcock-Crowe and the Meyer-Peter Müller sediment functions.

4.5.2. Evaluation of the model's performance

In order to evaluate the accuracy of each model's run, the model's results have to be compared with the field survey results, during the 2020 January flood. Thus, the results of the model were compared in terms of sediment volumes and in terms of geomorphological changes, namely the erosion and deposition patterns.

4.5.2.1. Correction of the DoD

The DoD stands for DTM of Difference and represents the subtraction of two DTMs, namely in this study the earlier DTM, minus the oldest. The DoD provides a spatial distribution and quantification of the depositional and erosion areas. Our modelling focuses on one of the floods on the Rambla de la Viuda in 2020, that occurred at the end of January 2020. Thus, the DoD cited in this section is composed of February 2020 DTM (post flood) minus the DTM of June 2019 (pre-flood) (Annexe 7). Hence, positive values represent deposition whereas negative values indicate erosion.

The methodology used to obtain the DTM was the photogrammetry. Without going into detail, this method is based on photographs taken from Unmanned Aerial Vehicles (UAVs). The pictures were taken from two points of view, allowing for the determination of the altitude at every location. However, the method is sensitive to the light conditions, and occasionally may introduce uniform errors that need some correction.

Knowing that, it is important to compute the Level of Detection (LOD), in order to apply a correction on the DoD. The first step to compute the LOD is to establish areas where it is certain that there has been no erosion or deposition. These areas were identified in the concrete road where we are confident that there is a fix ground. For instance, on the concrete road a gravel deposit can be accumulated, but in case that the DoD shows only erosion, it is evident that this represents a DTM's error. In addition, the paths outside the reach can be identified as stable areas, since those paths were not reached by the river flow. A point shapefile layer was created including those stable points. Then, the values of the DoD were extracted and entered into the point shapefile layer. In this way these points can be interpolated, taking the cell size of the DoD and its area. A raster is obtained following the interpolation, and by looking at the properties of it, the standard deviation must be collected and multiplied by two to get the LOD value.

Once the LOD value was known, the tool "Con" was used on ArcGIS to modify the values of the DoD following a condition. The aim was to remove all the values between the -LOD value and the +LOD value. Thus, the condition introduced in the "Con" tool, applied to the DoD, was as follows: if -LOD < VALUE < + LOD, the raster value must be changed to 0, otherwise, the value of the DoD must be retained (Annexe 8).

After the DoD was corrected from the LOD error, some systematic errors remained, especially at the upstream sector. There were numerous small patterns with huge values of deposition, which match with the trees, visible on the DTM and on orthophotographs. Nonetheless, these high deposition values do not correspond to any representative changes in sediment volume, but rather to changes in elevation linked to the vegetation of the trees. The vegetation growth and wind movements are a typical source of errors. In addition, the shade induced by the trees may not have been in the same place between the two DTM, leading to erroneous values in the DoD. A bar unit of the most upstream part also showed a uniform mean value of -10 centimetres. However, such uniform erosion over an extensive area is suspicious of being an error of the DoD, meaning that this area can be corrected.

The additional correction has been applied to the DoD, which consisted of setting to 0 the high deposit values belonging to trees, and the upstream and downstream bars areas. Then the final corrected DoD was obtained, which will be used to the comparison with the model results (Annexe 9).

4.5.2.2. Sediment volumes calculation

The bed change, corresponding to the elevation change in the bed in every cell of the mesh, was multiplied by the area of the cell to obtain the cell sediment volume variation. Finally, the sediment volume of each cell was summed to know the general sediment volume variation of each model's run.

Regarding the DoD sediment volume variation, the tool "Zonal statistics" in ArcGIS was used to estimate the mean variation in terms of bed elevation, in the upstream and the downstream parts. This value was multiplied by the area of the upstream and downstream parts of the reach to obtain the sediment volumes.

5. Results and discussion

5.1. Results

5.1.1. Capacity Ratio boundary condition

The figures 23 and 24 present the volumes obtained for each run using the capacity Ratio as upstream boundary condition, in comparison with the DoD deposition and erosion volumes recorded in the January 2020 flood. In the following figures, the upstream part refers to the part located upstream of the road and downstream part represents the part located downstream of the road.

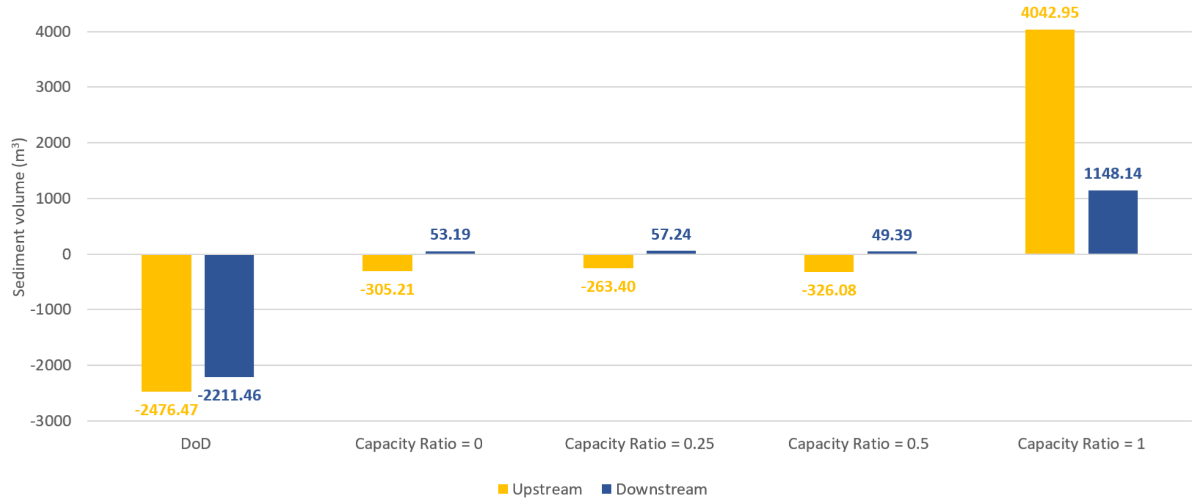

Figure 23: Sediment volumes after January 2020 flood, using Meyer-Peter Müller sediment function

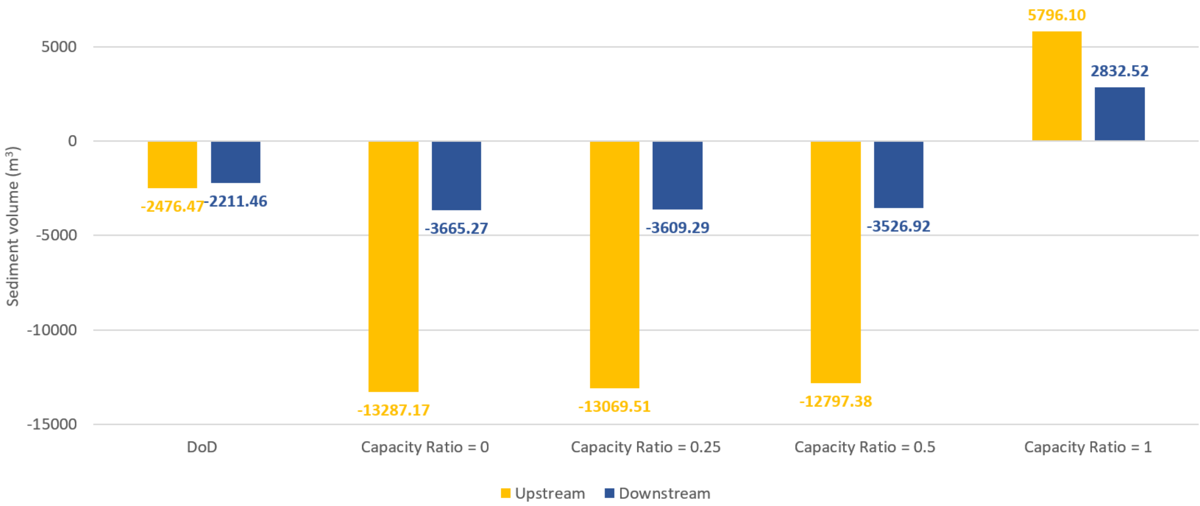

Figure 24: Sediment volumes after January 2020 flood peak, using Wilcock-Crowe sediment function

Regarding the volumes obtained with the Meyer-Peter Müller sediment function, the ones with a Capacity Ratio equal to 0, 0.25 and 0.5 represent well the erosion in the upstream part, but show a deposit downstream, which it is not the case for the DoD. For the Wilcock-Crowe sediment function, and the Capacity Ratios equal to 0, 0.25 and 0.5, both upstream and downstream parts present erosion. Nevertheless, the sediment volumes of the upstream part are particularly huge compared to the volumes of the DoD, with the model's values approximately equivalent to 32 times the volume of the DoD. Concerning the Capacity Ratio equal to 1, both sediment functions display an important deposit, upstream as well as downstream.

The computations with the Capacity Ratio have provided interesting results, notably for the Wilcock-Crowe sediment function. However, the results do not fit as much as expected the DoD figures.

5.1.2. Sediment Load Series boundary condition

Regarding the Sediment Load Series boundary condition, a sediment graph was entered for the upstream boundary condition. The results obtained in terms of volumes are shown in Figure 25 and those for the bed change in Annexe 10 and Annexe 11.

As the results obtained with the Capacity Ratio boundary conditions, the model gave closer volumes to the DoD with the Wilcock-Crowe sediment function. Although these results are not completely conclusive, due to the huge value of erosion in the upstream part. It can be explained by an insufficient amount of sediment input from the estimated sediment load series using the Recking equation.

Thereby, the sediment graph input has been multiplied by 2. The model using this sediment graph provided improved results, as the volume in the downstream part get closer to the DoD value. Regarding the upstream part, the volume obtained is still higher than the DoD one but get closer that previously.

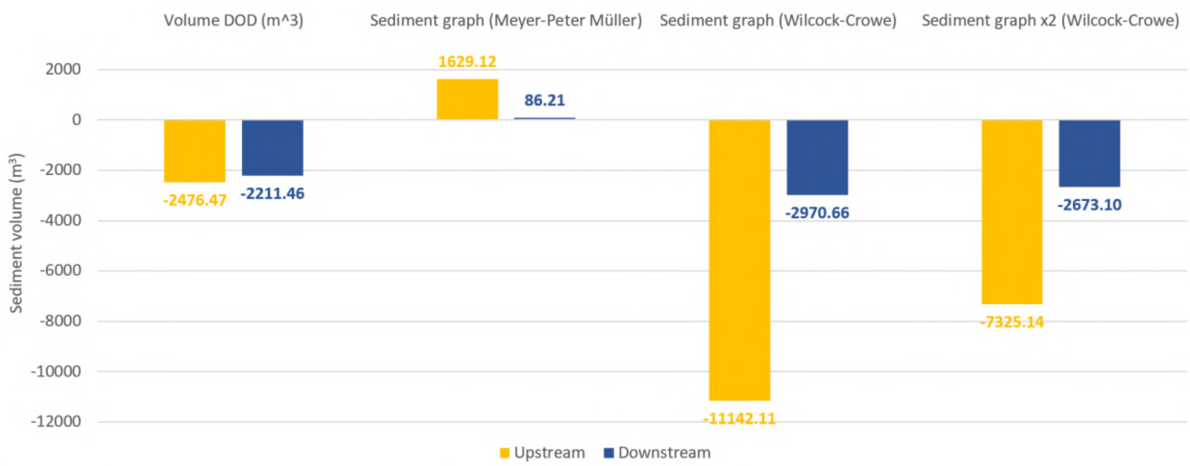

Figure 25: Sediment volumes after January 2020 flood peak, using Sediment graph as upstream boundary condition

The comparison between the DoD and the modelling results were done initially in terms of sediment volume, before examining the similarity between the geomorphologic changes, namely the location of the deposition and erosion areas. Thus, concerning the spatial variability of the deposition and erosion zones, the patterns are not strictly identical. As visible on the Figure 26, in the upstream part, there is a significant eroded part, located on a bar, that do not appear in the DoD. In addition, regarding the downstream part, there is also a large eroded area located on a bar just downstream the road, and this area is stable in the DoD. Overall, similar bed change pattern can be observed both in the model and in the DoD, although the model trend to extend the erosion areas likely due to the mesh resolution.

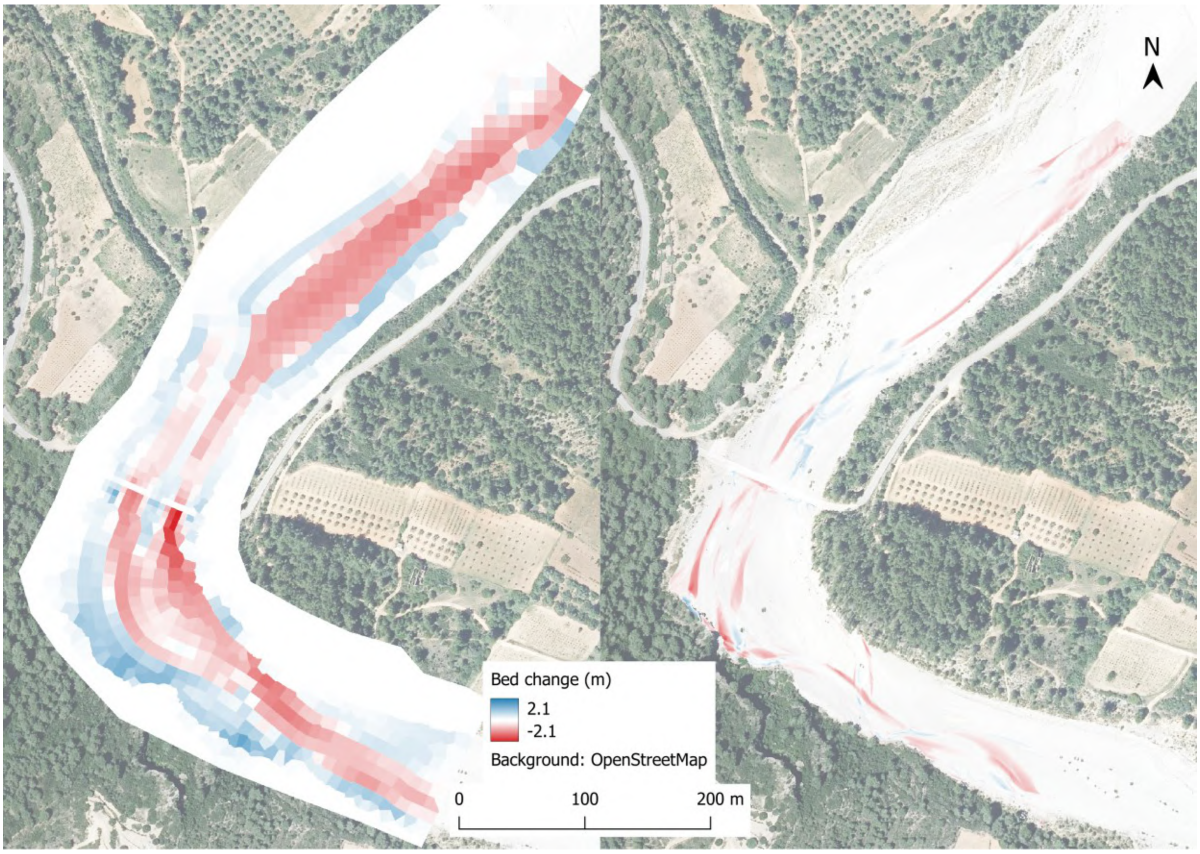

Figure 26: Geomorphologic comparison between the modelling with the Sediment graph multiplied by 2 (left) and DoD (right) (Source: L. Mesnil, 2024)

Moreover, the total bed load sediment flow at the downstream boundary condition was computed and estimated at 18,178 tonnes of sediment for the entire flood hydrograph, which corresponds to approximately 4,040 tonnes per day. In comparison, the total sediment input was 17,350 tonnes of sediment.

5.2. Discussion

The 2D HEC-RAS sediment modelling provided quite conclusive results. It gave coherent outcomes, that may represent well the morpho-sedimentary dynamics in the Rambla de la Viuda. It could be used for instance to estimate the duration and the water discharges required to fill with sediment a reach affected by in-stream gravel extraction. The model also showed a good performance in the estimation of the morpho-dynamics changes induced by gravel mining, which has an undeniable effect on morphological processes. Besides, the model has enabled to estimate the bed load sediment transport that flows through the reach.

To go further, it would be interesting to vary others parameters to see the influence on the models, starting with the number of model's runs. Given that the modelling computations take between 5 and 9 hours to run one model, it might be a good opportunity to exploit the use of Python on HEC-RAS, which enables the model's runs to be automated. This would allow a wider range of parameters to be tested and more precise results to be obtained, for instance to fit better the geomorphological changes.

6. Conclusion

In conclusion, the different steps carried out during the internship allowed to build a model which gives conclusive results. In this way, the particle size distribution for the surface and subsurface provided a good sediment spatial description in the model and improved the sediment flux and the spatial distribution of bed changes. In addition, the rating curve and the sediment load flux estimated by the Recking's question allowed to obtain the water discharges during the flood peak, essential to describe the boundary condition. Moreover, the corrections made to the DoD have provided a reliable reference against which to compare the model's results. Finally, this work has demonstrated the ability of 2D HEC-RAS modelling to estimate the bed load transport in ephemeral streams as well as to describe and represent the geomorphological changes.

On the other hand, I really benefited from this internship, because which I have learnt a lot by carrying out these numerous tasks. It also allowed me to discover the research domain, and to see how a research laboratory works. I was able to improve my knowledge in morpho-dynamics, 2D modelling on HEC-RAS, sedimentology, photogrammetry and to better my English skills, especially regarding the report writing.

7. Bibliography

Bizzi, B Blamauer, G Braca, M Bussettini, B Camenen, F Comiti, L Demarchi, D. García De Jalón, M. Gonzàles Del Tànago, R.C. Grabowski, A.M. Gurnell, H. Habersack, B. Lastoria, A. Latapie, V. Martìnez-Fernàndez, J.O. Mountford, L. Nardi, M.T. O'Hare, C. Percopo, … L. Ziliani. (2014). Thematic Annexes of the Multi-scale Hierarchical Framework. REFORM (REstoring rivers FOR effective catchment Management), a Collaborative project (large-scale integrating project) funded by the European Commission within the 7th Framework Programme under Grant Agreement 282656. https://doi.org/10.13140/2.1.1913.2489

Bunte, K., & Abt, S. R. (2001). *Sampling surface and subsurface particle-size distributions in wadable gravel-and cobble-bed streams for analyses in sediment transport, hydraulics, and streambed monitoring* (RMRS-GTR-74; p. RMRS-GTR-74). U.S. Department of Agriculture, Forest Service, Rocky Mountain Research Station. https://doi.org/10.2737/RMRS-GTR-74

Camarasa Belmonte, A. M., & Segura Beltrán, F. (2001). Flood events in Mediterranean ephemeral streams (ramblas) in Valencia region, Spain. *CATENA*, *45*(3), 229-249. https://doi.org/10.1016/S0341-8162(01)00146-1

Church, M.A., McLean, D.G., Wolcott, J.F., (1987). River Bed Gravels: Sampling and Analysis. In: Thorne, C.R., Bathurst, J.C., Hey, R.D. (Eds.), Sediments transport in Gravel Bed Rivers. John Wiley and Sons, New York, pp. 43–88.

Gallart, F., Cid, N., Latron, J., Llorens, P., Bonada, N., Jeuffroy, J., Jiménez-Argudo, S.-M., Vega, R.-M., Solà, C., Soria, M., Bardina, M., Hernández-Casahuga, A.-J., Fidalgo, A., Estrela, T., Munné, A., & Prat, N. (2017). TREHS : An open-access software tool for investigating and evaluating temporary river regimes as a first step for their ecological status assessment. *Science of The Total Environment*, *607-608*, 519-540. https://doi.org/10.1016/j.scitotenv.2017.06.209

Gómez, R., Hurtado, I., Suárez, M. L., & Vidal-Abarca, M. R. (2005). Ramblas in south-east Spain : Threatened and valuable ecosystems. *Aquatic Conservation: Marine and Freshwater Ecosystems*, *15*(4), 387-402. https://doi.org/10.1002/aqc.680

HEC-RAS 2D Sediment Transport Technical Reference Manual. (w.d). Meyer-Peter and Müller. Consulted on 8 July 2024 at https://www.hec.usace.army.mil/confluence/rasdocs/d2sd/ras2dsedtr/latest/model-description/transport-potential-formulas/meyer-peter-and-mueller

HEC-RAS 2D Sediment Transport Technical Reference Manual. (w.d). Wilcock and Crowe. Consulted on 8 July 2024 at https://www.hec.usace.army.mil/confluence/rasdocs/d2sd/ras2dsedtr/latest/model-description/transport-potential-formulas/wilcock-and-crowe

HEC-RAS 2D Sediment Transport Technical Reference Manual. (w.d). Hiding and Exposure Corrections. Consulted on 8 July 2024 at https://www.hec.usace.army.mil/confluence/rasdocs/d2sd/ras2dsedtr/latest/model-description/hiding-and-exposure-corrections

HEC-RAS 2D Sediment Transport Technical Reference Manual. (w.d). Particle Settling Velocity. Consulted on 8 July 2024 at https://www.hec.usace.army.mil/confluence/rasdocs/d2sd/ras2dsedtr/latest/model-description/fall-velocity-and-settling/particle-settling-velocity

HEC-RAS Water Quality Technical Reference. (2018). The Courant Number. https://www.hec.usace.army.mil/software/hec-ras/documentation/HEC-RAS%20Water%20Quality%20Technical%20Reference-v6.4.1.pdf

López, R., Ville, F., Garcia, C., Batalla, R. J., & Vericat, D. (2023). Bed-material entrainment in a mountain river affected by hydropeaking. Science of The Total Environment, 856, 159065. https://doi.org/10.1016/j.scitotenv.2022.159065

Museo Nacional de Ciencias Naturales. (w. d.). Presentación. Consulted on 17 June 2024 at https://www.mncn.csic.es/es

Recking A. (2017, mars 01). ELEMENTS DE GEOMORPHOLOGIE FLUVIALE, Cahier 2 : La granulométrie des cours d'eau (et sa mesure). Consulted on 16 May 2024 at https://www.bedloadweb.com/Granulometrie.pdf

Skoulikidis, N. T., Sabater, S., Datry, T., Morais, M. M., Buffagni, A., Dörflinger, G., Zogaris, S., Del Mar Sánchez-Montoya, M., Bonada, N., Kalogianni, E., Rosado, J., Vardakas, L., De Girolamo, A. M., & Tockner, K. (2017). Non-perennial Mediterranean rivers in Europe : Status, pressures, and challenges for research and management. *Science of The Total Environment*, *577*, 1-18. https://doi.org/10.1016/j.scitotenv.2016.10.147

Stanford G. (2021, april 12). *Align Cells with Flow Direction: HEC-RAS 2D Mesh* [Video]. YouTube. https://www.youtube.com/watch?v=oTfFdSmXbYQ

Vázquez-Tarrío, D., Piégay, H., & Menéndez-Duarte, R. (2020). Textural signatures of sediment supply in gravel-bed rivers : Revisiting the armour ratio. Earth-Science Reviews, 207, 103211. https://doi.org/10.1016/j.earscirev.2020.103211

Vázquez-Tarrío, D., Piqué, G., Vericat, D., & Batalla, R. J. (2021). The active layer in gravel-bed rivers: An empirical appraisal. Earth Surface Processes and Landforms, 46(2), 323-343. https://doi.org/10.1002/esp.5027

Wolman, M. G. (1954), A method of sampling coarse river-bed material, Eos Trans. AGU, 35(6), 951–956, https://doi.org/10.1029/TR035i006p00951

8. Annexes

Annexe 1: Orthophotograph with improved colours in the study site

Annexe 2: Digital Terrain Model (Source: Hydrology and Climate Change Laboratory, 2019)

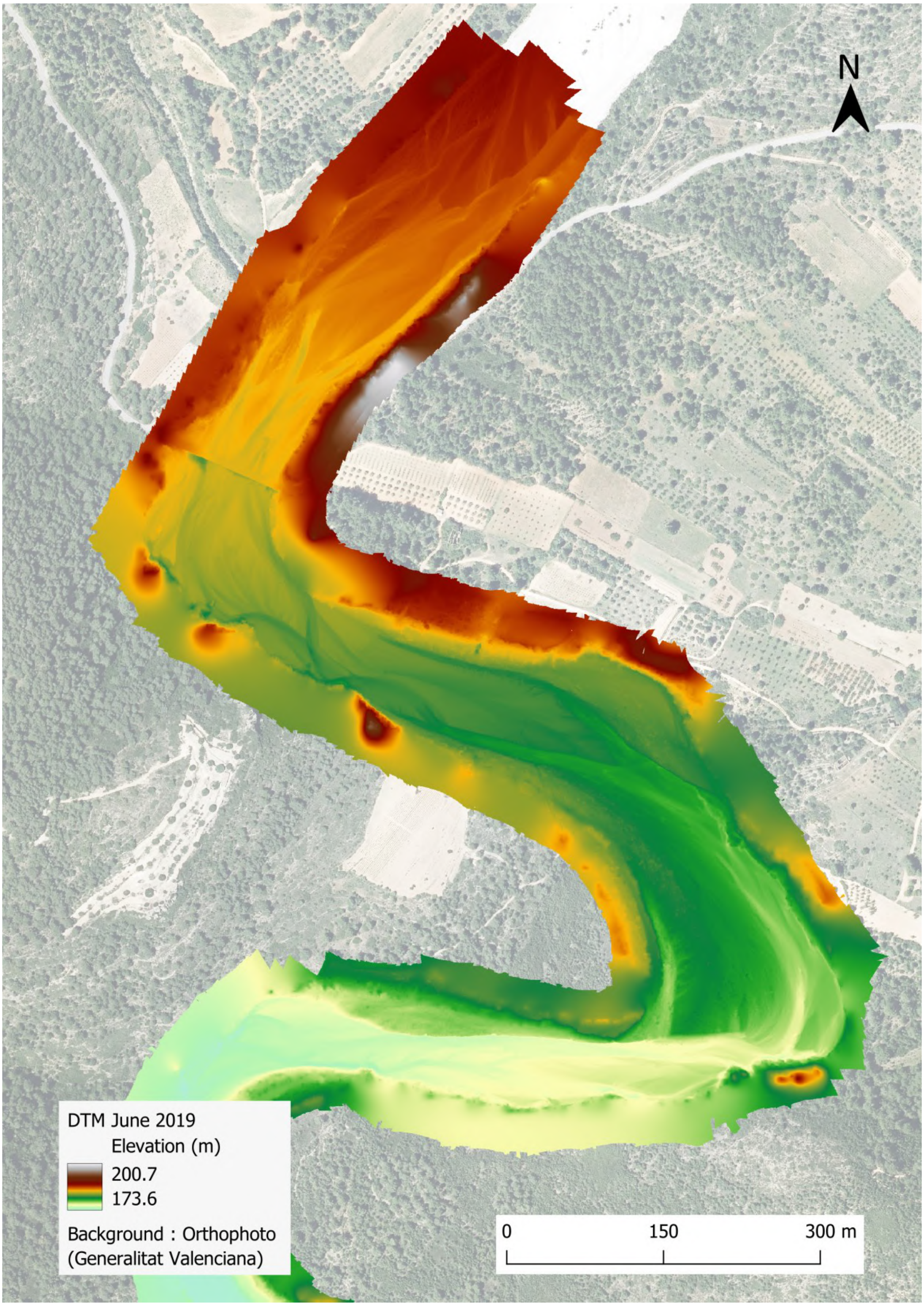

Annexe 3: Digital Terrain Model with shades (Source: Hydrology and Climate Change Laboratory, 2019)

<u>Annexe 4 :</u> Geomorphological mapping (Source: L. Mesnil, 2024)

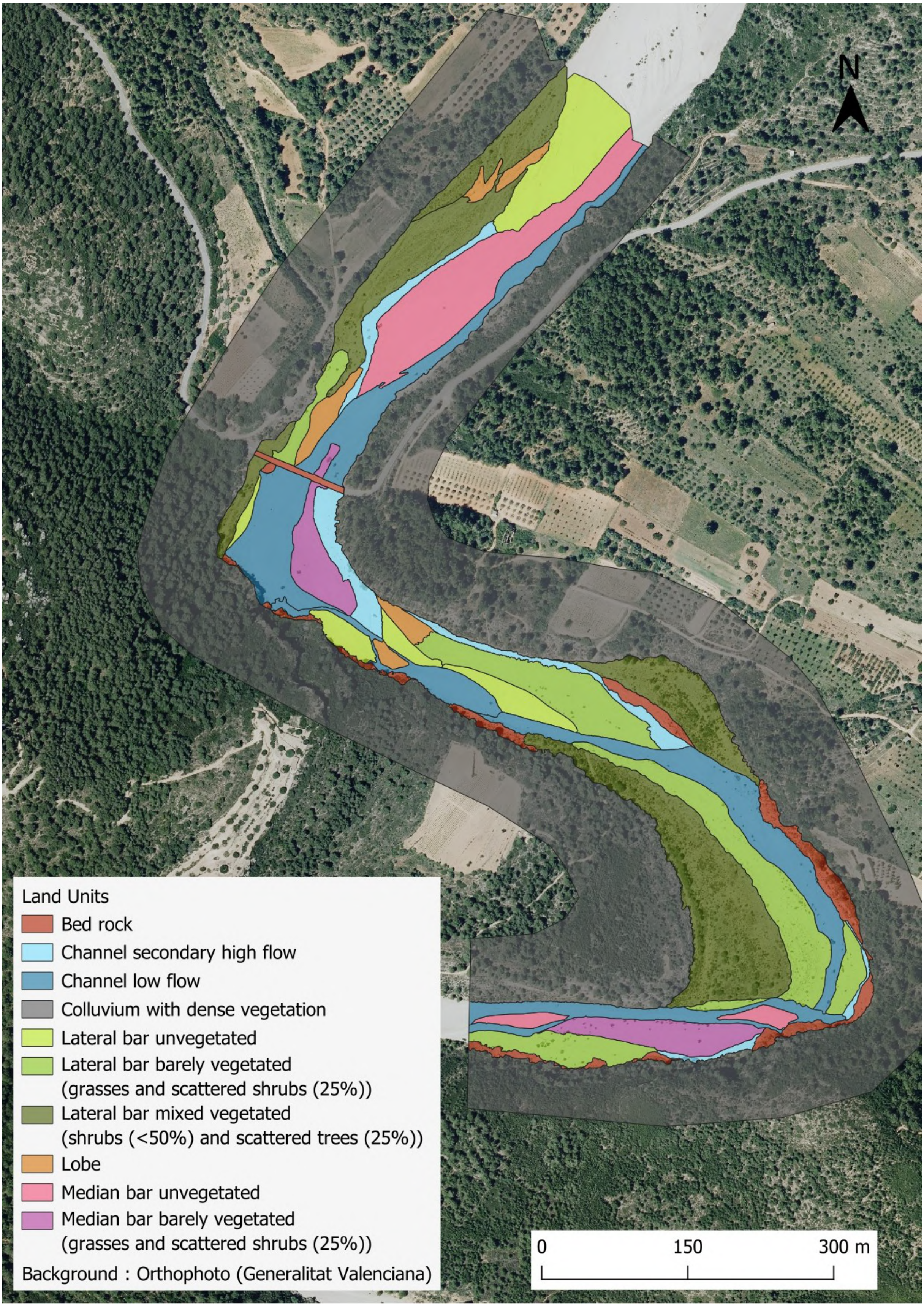

Annexe 5: Manning's values (Source: L. Mesnil, 2024)

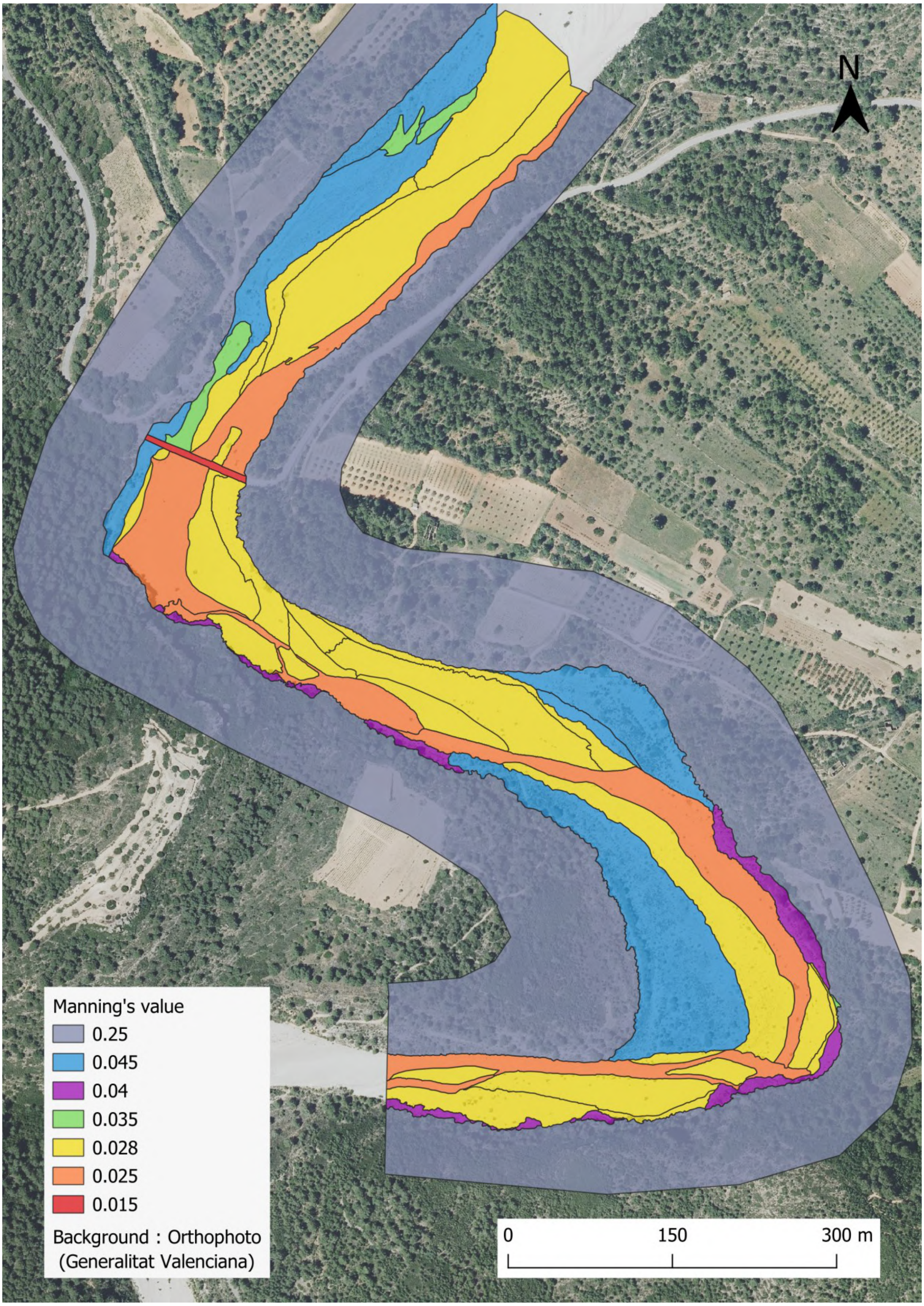

Annexe 6: Model mesh (Source: L. Mesnil, 2024)

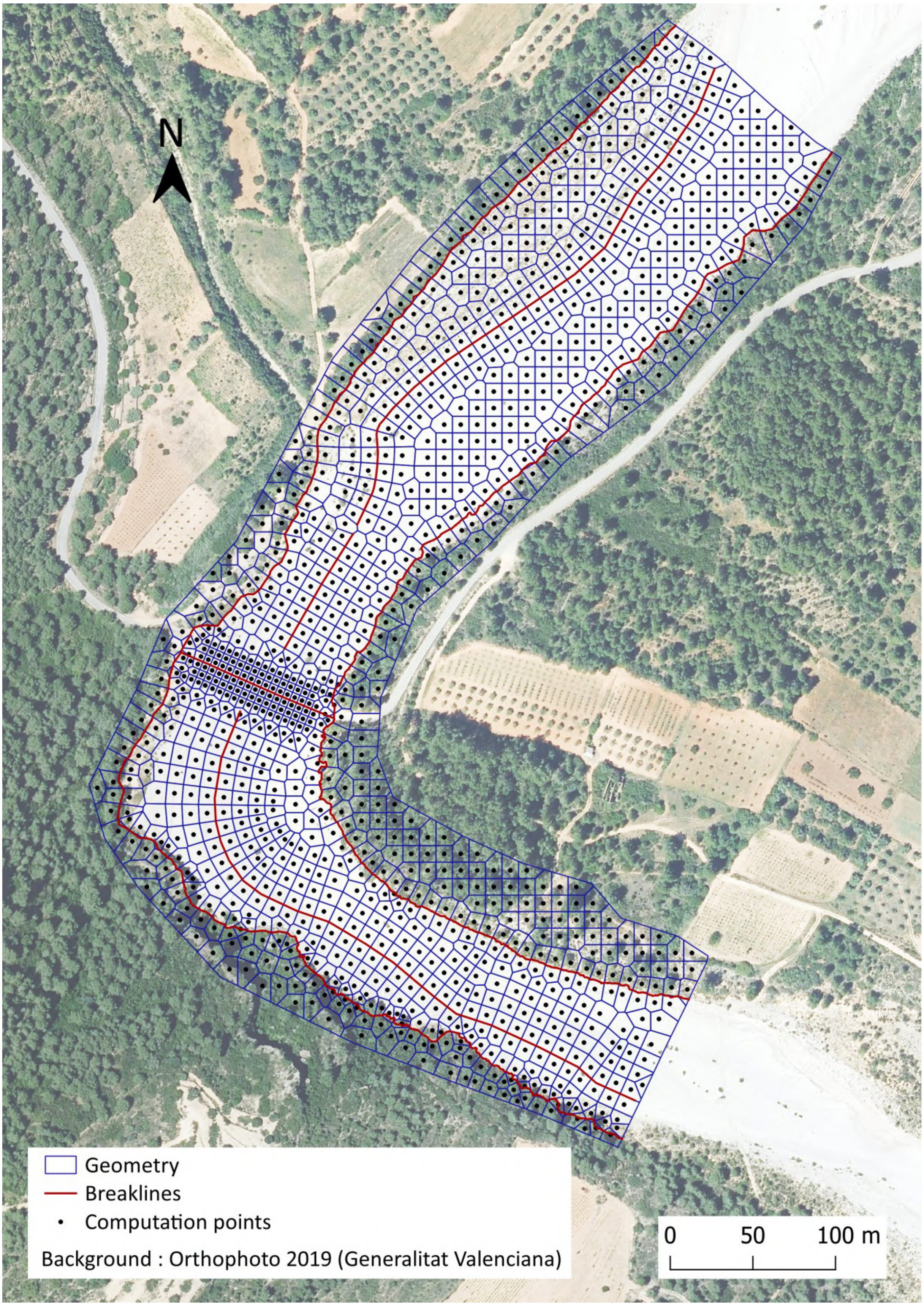

Annexe 7: Raw DoD (Source: L. Mesnil, 2024)

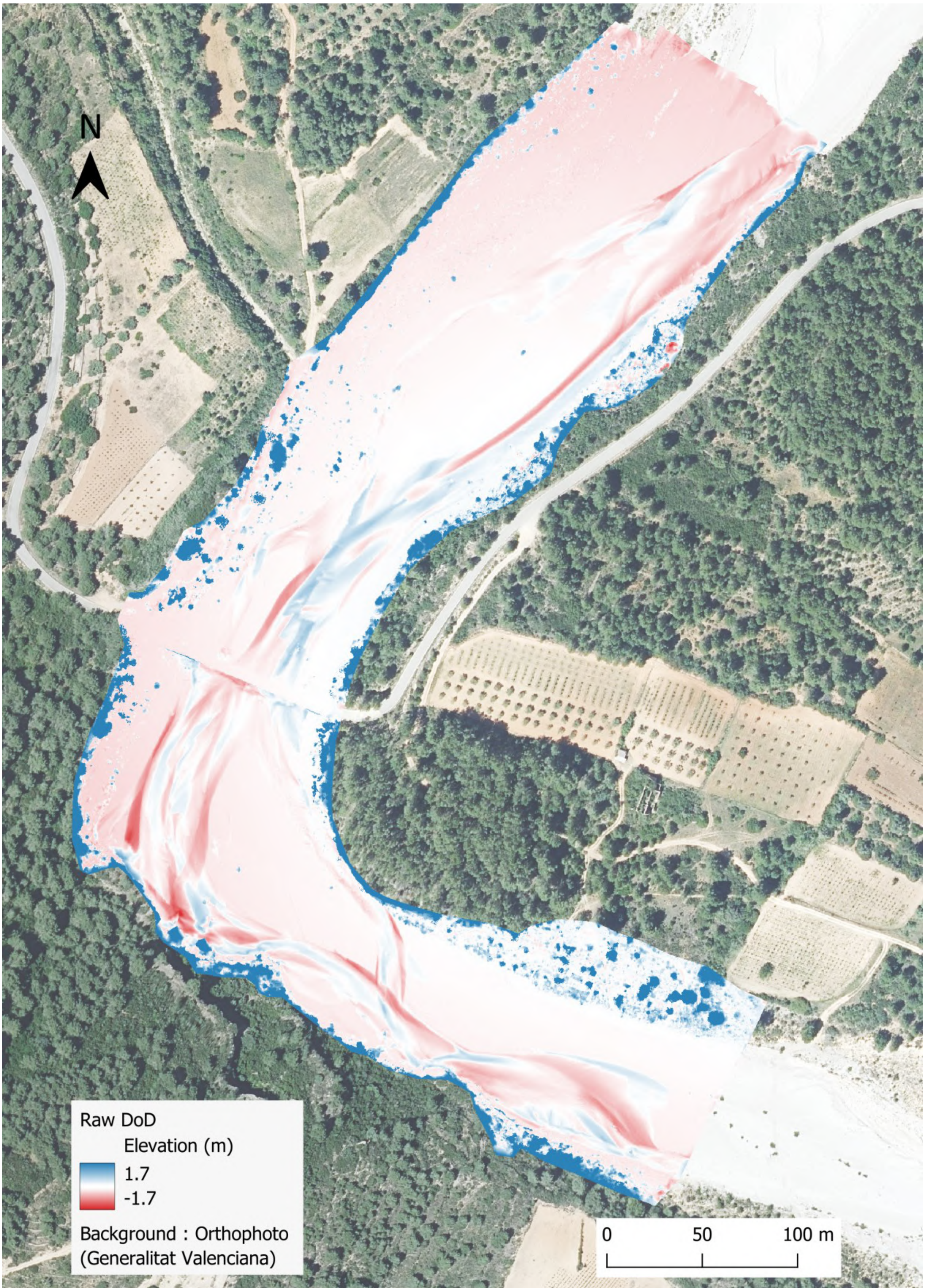

Annexe 8: DoD corrected with the LOD (Source: L. Mesnil, 2024)

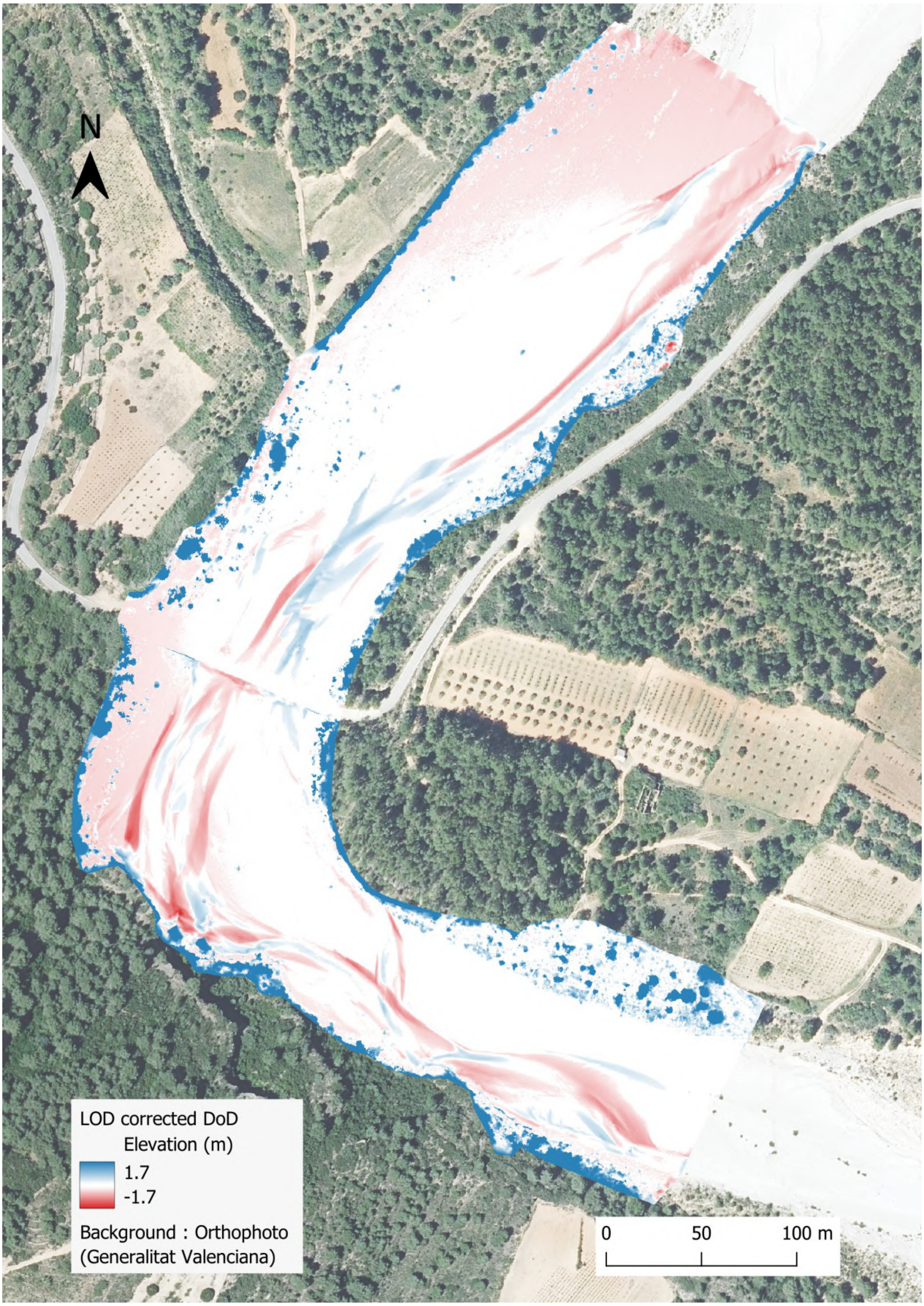

Annexe 9: Corrected DoD (Source: L. Mesnil, 2024)

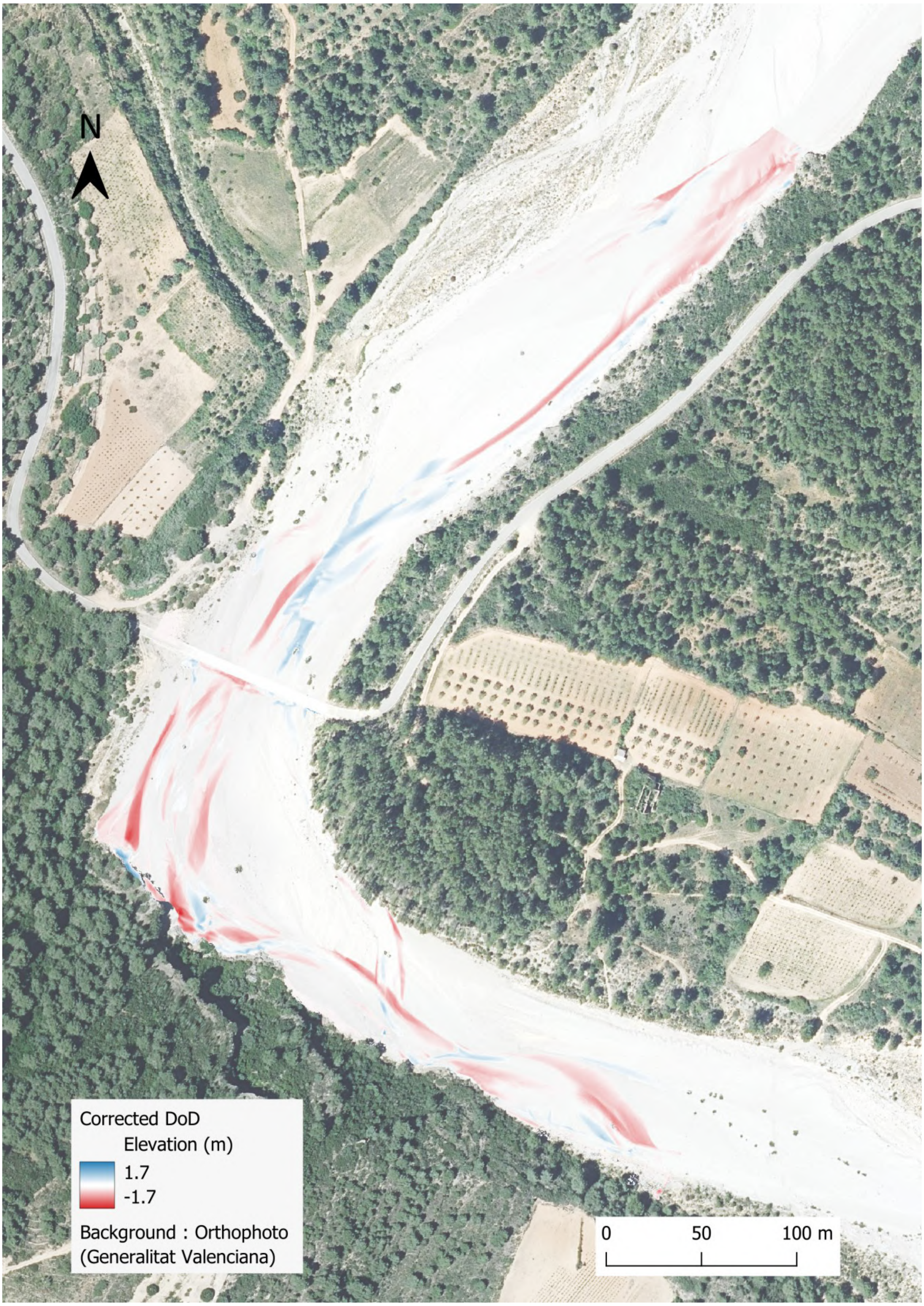

Annexe 10: Bed change with Sediment graph input (Source: L. Mesnil, 2024)

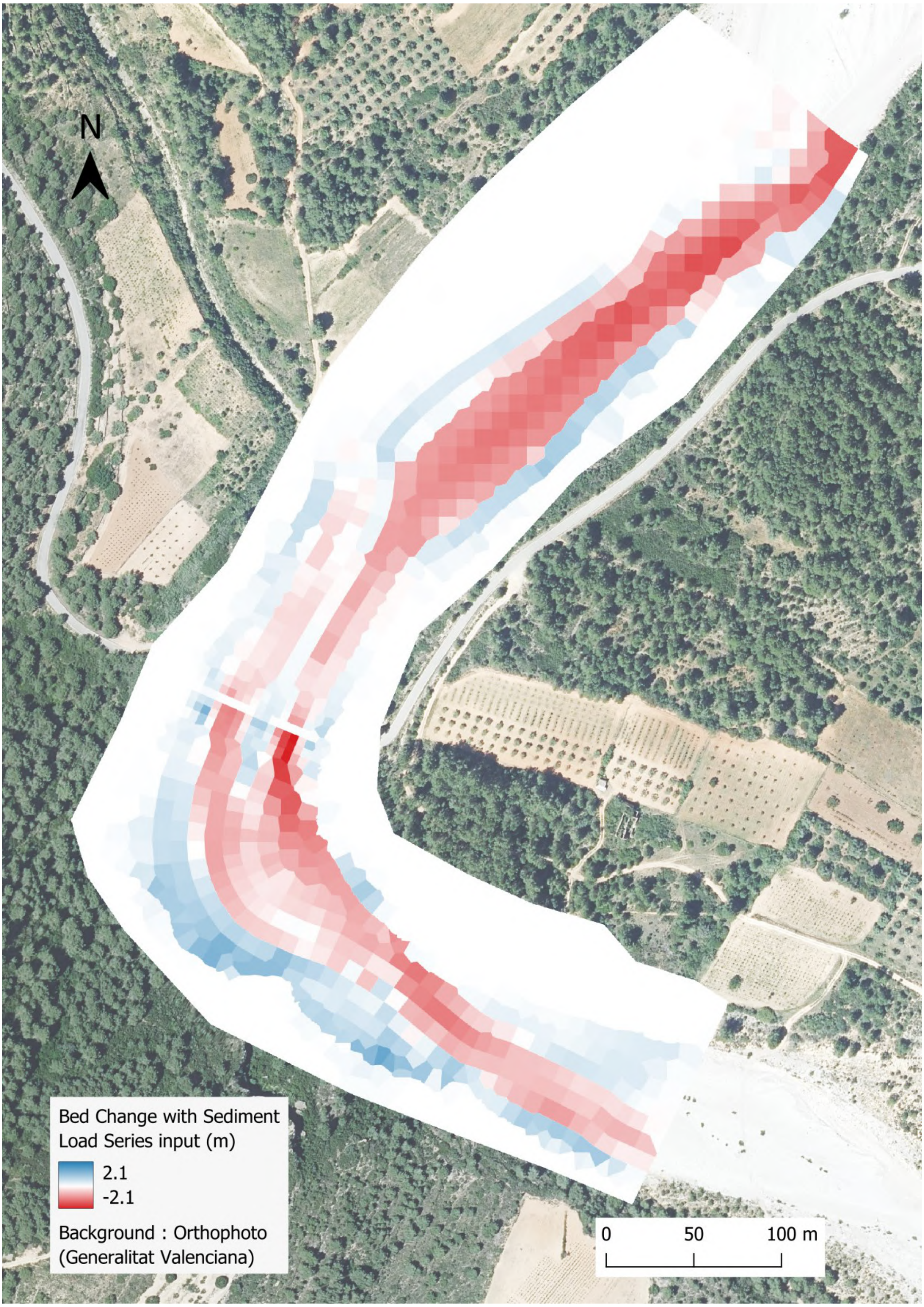

Annexe 11: Bed change with Sediment graph input multiplied by 2 (Source: L. Mesnil, 2024)

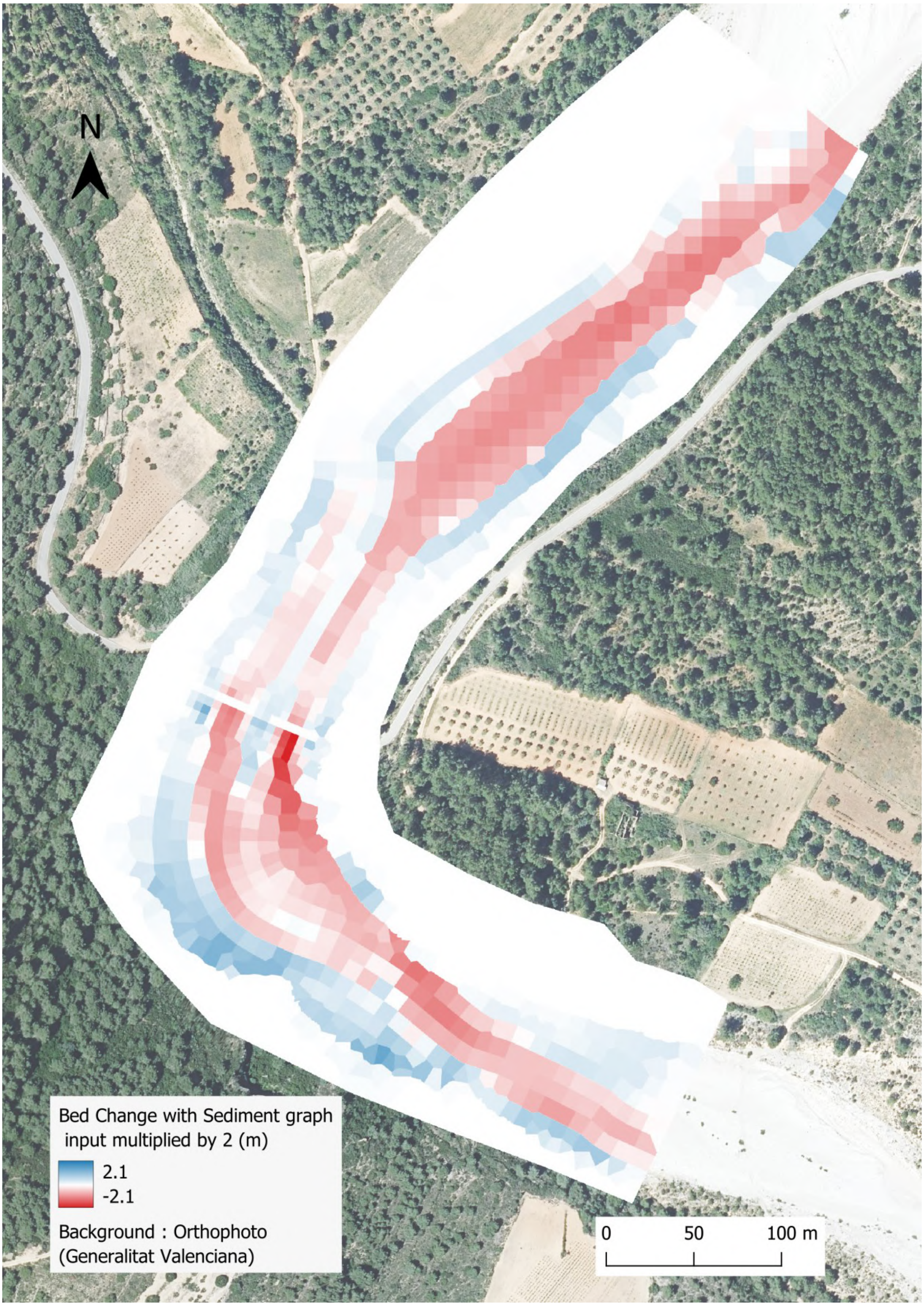

35 ALLÉE FERDINAND DE LESSEPS
37200 TOURS

Léa Mesnil
2023-2024

Analysis of morpho-sedimentary dynamics of a Mediterranean stream affected by human disturbance

Résumé :
This internship was carried out at the Hydrology and Climate Change research laboratory, and has focused on the Rambla de la Viuda, a Mediterranean ephemeral stream. The aim was to model the sedimentary transport and geomorphology changes along the stream, after a flood peak, using a 2D modelling on HEC-RAS.

Key Words: HEC-RAS 2D modelling, hydraulics, sedimentology, grain size distribution, hydromorphology

Museo Nacional de Ciencias Naturales (MNCN) - CSIC
C. de José Gutiérrez Abascal, 2, 28006 Madrid, Spain

Tuteur entreprise :
Gerardo Benito
Researcher/ Professor

Tuteur académique :
Stéphane Rodrigues